Robust Power Loading for the TDD MISO Downlink with Outage Constraints

ROBUST POWER LOADING FOR THE TDD MISO DOWNLINK WITH OUTAGE CONSTRAINTS

BY

FOAD SOHRABI, B.Sc.

A THESIS

SUBMITTED TO THE DEPARTMENT OF ELECTRICAL & COMPUTER ENGINEERING

AND THE SCHOOL OF GRADUATE STUDIES

OF MCMASTER UNIVERSITY

IN PARTIAL FULFILMENT OF THE REQUIREMENTS

FOR THE DEGREE OF

MASTER OF APPLIED SCIENCE

Master of Applied Science (2013) McMaster University

(Electrical & Computer Engineering) Hamilton, Ontario, Canada

TITLE:	Robust Power Loading for the TDD MISO Downlink with Outage Constraints
AUTHOR:	Foad Sohrabi B.Sc., (Electrical Engineering) University of Tehran, Tehran, Iran
SUPERVISOR:	Dr. T. N. Davidson
NUMBER OF PAGES:	xiii, 88

To my beloved wife:

Mahsa

Abstract

We consider the problem of power allocation for the single-cell multiple-input single-output (MISO) downlink in a time division duplex (TDD) system. In such systems, the base station (BS) acquires information about the channel state during the training component of the uplink phase. The resulting estimation errors are modeled probabilistically, and the receivers specify quality-of-service (QoS) constraints in terms of a target signal-to-interference-and-noise ratio that is to be achieved with a given outage probability. For a fixed beamforming structure, we seek a power allocation that minimizes the transmission power required to satisfy the users' QoS requests.

The proposed approach to that problem begins with the observation that for TDD systems the channel estimation error at the base station can be modeled as being additive and Gaussian. Under that model, we obtain a precise deterministic characterization of the outage probability, and mildly conservative approximations thereof. Although the resulting deterministic optimization problems are not convex, we have been able to obtain good solutions using straightforward coordinate update algorithms. In fact, these solutions provide significantly better performance than the existing approaches, which are based on convex restrictions, because the proposed approximations are less conservative. By developing some approximations of the precise deterministic characterization of the outage probability, we develop algorithms

that have good performance and much lower computational cost.

Acknowledgements

I would like to express my deepest appreciation and gratitude to my supervisor Prof. Tim Davidson for his excellent guidance, caring, constructive supervision and his patience in reviewing ideas, papers and this thesis. Without his encouragement and effort this thesis would not have been completed.

I am deeply grateful to Prof. Wong and communication research group for providing motivative seminars and constructive discussions within the group.

Special thanks to Electrical and Computer Engineering Department administrative team for their help in many matters.

Last but not least, I would like to thank my family for their endless love and for always supporting me through the highs and lows of my life. I owe my deepest gratitude to my wonderful colleague and beautiful wife, Mahsa, for her brilliant ideas, encouragement, kindness and love. I am also deeply indebted to my parents for their unconditional support, both financially and emotionally throughout my life.

Abbreviations

BS	Base Station
CDF	Cumulative Distribution Function
CSI	Channel State Information
FDD	Frequency Division Duplex
MIMO	Multiple-Input Multiple-Output
MISO	Multiple-Input Single-Output
QoS	Quality-of-Service
RAR	Relaxation and Restriction
RCI	Regularized Zero-Forcing
RPL	Robust Power Loading
RV	Random Variable
SDP	Semidefinite Program
SINR	Signal-to-Inteference-and-Noise-Ratio
SNR	Signal-to-Noise-Ratio
SOCP	Second-Order Cone Program
TDD	Time Division Duplex
UT	User Terminal
ZF	Zero-Forcing

Contents

List of Figures

Chapter 1

Introduction

Communication systems can be classified into the classes of wireline systems, in which wires or other infrastructure are used to guide the propagation from transmitter to receiver, and wireless systems in which no such infrastructure is provided and the paths of propagation are determined by the nature of the environment. Perhaps the most prominent advantage of wireless communication systems over traditional wireline systems is the ability to communicate even when the transmitters are mobile. In addition, wireless systems rely far less on installed infrastructure, and hence wireless networks can be installed quickly and comparatively cheaply. Furthermore, the wireless medium is fundamentally a broadcast medium that enables simultaneous communication with multiple users. However, that advantage raises the challenge of managing interference. In contemporary wireless networks, this is done by dividing a geographical region into cells, with each cell being served by a single fixed-location transceiver known as a base station, or access point. The basic idea behind the division into cells is to ensure that neighbouring cells operate in different frequency bands. This means that the dominant sources of interference lie within each cell. Since the

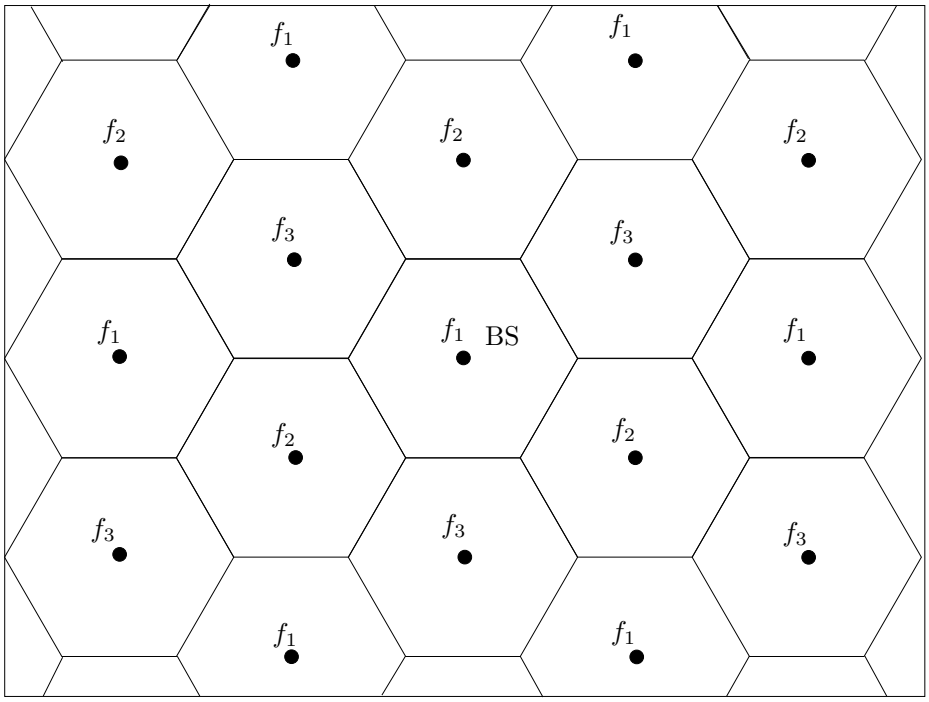

Figure 1.1: A schematic of a cellular system, with the center frequency of each cell indicated.

(average) power from an interfering source decays quite quickly with distance, frequency bands can be reused in cells that are sufficiently well separated. A schematic diagram of a typical cellular network is illustrated in Fig. 1.1. (In the figure, the cells are uniformly hexagonal, but that is not always the case in practice.) This diagram illustrates the fact that although the partition of the region into cells reduces the task of interference management to interference management within each cell, it does leave some bands idle in certain geographical areas. There have been a number of research proposals that suggest that interference can be managed over multiple cells and hence the number of idle bands can be reduced (e.g., Gesbert *et al.*, 2010). However, the focus of this thesis is on cellular networks that operate on a cell-by-cell basis.

In a conventional cellular network, there are two main tasks within a cell: downlink communication, which is communication from base station to mobile; and uplink communication, which is communication from mobile to base station. The operations on the downlink and uplink are separated in time or frequency. In frequency-division duplexed (FDD) systems, the transmitter and receiver operate in different bands, whereas in time-division duplexed (TDD) systems, the uplink is separated from downlink by allocation of different time slots in the same frequency band. The main focus of this thesis will be on the downlink of TDD systems.

In a wireless medium, objects in the environment reflect or scatter the transmitted signal and create different paths along which the transmitted signal propagates to the receiver. As a result, the received signal is a superposition of different copies of transmitted signal that experience different channels with different attenuation, delay and phase shift. Furthermore, the attenuation, delay and phase shift change with the positions of the transmitter, receiver and scatterers. The combined effect of those changes is known as fading.

In the sense of the rate of the changes in the channel gains, we can consider two broad classes of fading, fast fading and slow fading. In order to distinguish fast fading and slow fading channels, we define a parameter called the coherence time. The coherence time is the time duration in which the channel gain remains approximately constant. Slow fading arises when the coherence time is larger than duration of transmitted signal, which means that the channel can be considered to be constant during transmission. On the other hand, when the channel varies significantly during the transmission that means the coherence time is smaller than signal duration, and the channel is said to be a fast fading channel.

The other classification of fading is based on the notion of coherence bandwidth. The coherence bandwidth is a measurement of the maximum frequency interval over which the channel remains approximately constant. The first class is the flat fading channel, in which the coherence bandwidth is larger than the bandwidth of the transmitted signal. Hence, all frequency components of the transmitted signal experience the same channel. If the coherence bandwidth is smaller than the bandwidth of the signal, different frequency components of the transmitted signal experience different channel conditions. In that case, channel is said to be a frequency-selective fading channel.

Throughout this thesis, we will consider a frequency-flat block-fading channel in which the channel is assumed to remain constant over a block-length and change between different blocks. This means that the channel is modeled as being constant over each block. This class of channels is appropriate for wide range of wireless communication (Tse and Viswanath, 2005; Goldsmith, 2005).

1.1 Linear Downlink Precoding in Wireless Communication

The focus of this thesis is on downlink transmission, from the base station to mobile users, as illustrated in Fig. 1.2. In the considered model, the base station has N_t antennas and each of the K users has a single antenna. Such schemes are often said to be multi-user multiple-input single-output (MISO) systems. The base station's goal is to send, simultaneously, an independent message to each of the K receivers. To do so, it constructs a suitable coding scheme. In the case in which the BS has

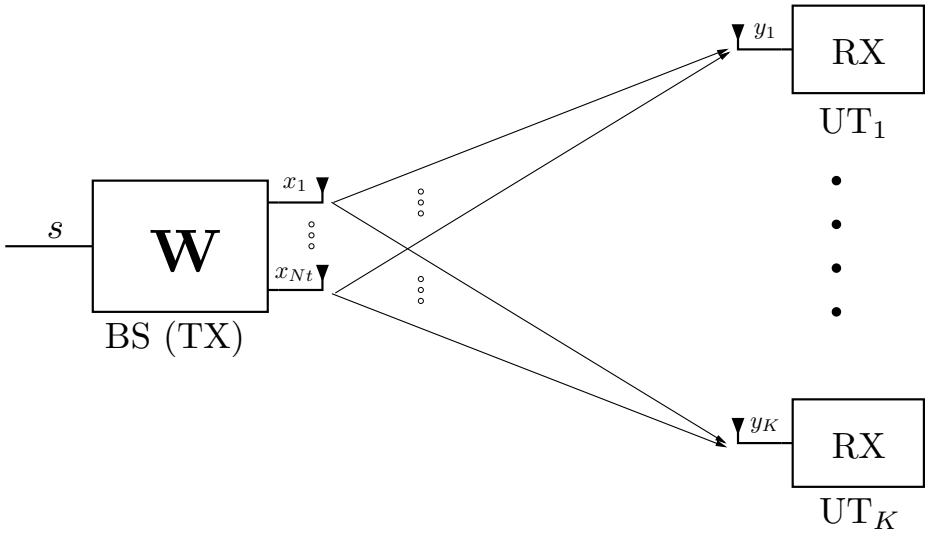

Figure 1.2: A single-cell downlink setting with N_t antennas at the base station (BS) and K users, each with a single antenna.

perfect knowledge of the state of each the channels, the dirty paper coding scheme is optimal in the sense it enables the system to achieve any rate tuple in the capacity region (Caire and Shamai, 2003; Weingarten *et al.*, 2006). However, that scheme is based on the principle of pre-subtraction of the interference that the base station knows it will induce at the receivers, and is quite complicated to implement. As a result simpler sequential interference pre-subtraction schemes, such as those based on Tomlinson-Harashima precoders (Windpassinger *et al.*, 2004; Fung *et al.*, 2007; Liu and Krzymien, 2008) and vector perturbation precoding (Hochwald *et al.*, 2005), and even simpler schemes based on linear precoding (Spencer *et al.*, 2004; Bengtsson and Ottersten, 2001), have been adopted.

The focus of this thesis is on schemes based on linear precoding, in which each massage is independently encoded, and at each channel use the transmitter sends a signal from each of its antennas that is a linear combination of a symbol from the codeword of each user. In the notation in Fig. 1.2, if we let $\mathbf{s} = [s_1, s_2, \ldots, s_K]^T$

denote a vector containing one symbol from each codeword, then the transmitted signal can be written as $\mathbf{x} = \mathbf{W}\mathbf{s}$. If we let $\mathbf{w}_k$ denote the k^{th} column of $\mathbf{W}$, we can write $\mathbf{x} = \sum_{k=1}^{K} \mathbf{w}_k s_k$, which highlights the fact that each symbol can be viewed as modulating a beamformer $\mathbf{w}_k$ that is directed towards user k. The key task in downlink linear precoding is to design the downlink precoding matrix $\mathbf{W}$.

In some wireless communication applications, $\mathbf{W}$ is designed to maximize some measure of total throughput, i.e., the sum performance or the minimum of the achievable rates of each user, where the power resources are the constraints. On the other hand, in some applications fixed-rate traffic is required. In this case, the precoder is often designed so as to minimize the power consumption at the transmitter that is required to enable reliable communication to each receiver at specific target rate (e.g., Rashid-Farrokhi *et al.*, 1998; Bengtsson and Ottersten, 2001).

In order to design the precoding matrix, the BS must adapt to the channel conditions; if it does not, or cannot because it does not have information regarding the channel conditions, then the performance is degraded due to inter-user interference (Gesbert *et al.*, 2007; Jindal, 2006). For example, in the presence of additive white Gaussian noise at the receivers, if the BS has perfect channel state information (CSI), then the sum of the ergodic achievable rates grows as $\min(N_t, K)\log(\mathsf{SNR})$ as the SNR increases, where SNR is the signal-to-noise ratio. However, in the absence of CSI, the sum rate grows only as $\log(\mathsf{SNR})$ as the SNR increases. This means that in the absence of CSI at the transmitter, the sum rate is the same as the sum rate of a system with a single transmit antenna (Jindal, 2006).

The acquisition of channel state information at the transmitter is dependent on the structure of communication system. In FDD systems, the channel is estimated

at each user terminal (UT) and each UT feeds this estimate back the BS. In TDD systems, the reciprocal nature of the channel is exploited and the channel is estimated during the time interval when the direction of communication is reversed. As will be explained in Chapter 2, the focus of this thesis is on TDD systems.

In the discussion so far, we have presumed that the users to which the BS will transmit have been predetermined. In practice, this is done with a scheduling algorithm that is aware of the CSI of the users, the state of the queues of the users, the service priorities of the users, and the goals of the system operator. Most of development in this thesis is independent of the choice of the scheduling algorithm, but in Chapter 5 we will demonstrate the interaction with scheduling algorithms.

1.2 Brief Literature Review

It has long been recognized that the provision of multiple antennas at the transmitter of a downlink system has the potential to significantly improve the efficiency with which messages can be communicated; (e.g., Winters *et al.*, 1994; Weingarten *et al.*, 2006; Gesbert *et al.*, 2007). In the case of fixed-rate traffic, one way in which that potential can be realized is to design a linear transmitter so as to minimize the power that is required to enable reliable communication to each receiver at their specified target rate; (e.g., Rashid-Farrokhi *et al.*, 1998; Bengtsson and Ottersten, 2001). For narrowband systems in which the receivers have a single antenna, that quality-of-service (QoS) problem is equivalent to minimizing the transmission power required to satisfy a signal-to-interference-and-noise (SINR) constraint at each receiver; (e.g., Rashid-Farrokhi *et al.*, 1998; Bengtsson and Ottersten, 2001); i.e., $\min \mathsf{power}$ subject to $\mathsf{SINR}_k \geq \gamma_k$. Although linear transmitters are not optimal for

that problem (Weingarten *et al.*, 2006), they are relatively simple to implement. Under the assumption that the transmitter can be provided with accurate CSI, without expending a significant fraction of the channel resources, optimal linear precoders for a variety of such quality-of-service (QoS) problems have been obtained; (e.g., Bengtsson and Ottersten, 2001; Wiesel *et al.*, 2006; Schubert and Boche, 2007; Hunger and Joham, 2010; Huang and Palomar, 2010).

In practice, however, the CSI that can be made available at the transmitter is imperfect, due to estimation errors, quantization, feedback delay, feedback errors, and other effects; (e.g., Caire *et al.*, 2010). A prudent approach for dealing with the resulting uncertainty in the CSI is to incorporate a model for the uncertainty into the transmitter design. One approach to doing so is to adopt a bounded model for the uncertainty and to design a transmitter that satisfies the QoS requirements even for the worst case of the uncertainties admitted by the model; i.e., $\min \mathsf{power}$ subject to $\mathsf{SINR}_k \geq \gamma_k$ for all uncertainties; (e.g., Botros Shenouda and Davidson, 2007; Zheng *et al.*, 2008; Vucic and Boche, 2009; Botros Shenouda and Davidson, 2009). In this thesis we will consider an alternative approach in which the uncertainty is modeled probabilistically, and the QoS requirements are to be satisfied up to a given probability of outage; i.e, $\min \mathsf{power}$ subject to $\Pr(\mathsf{SINR}_k \geq \gamma_k) \geq 1 - \epsilon_k$. Several techniques for finding good linear precoders for such problems have been developed (Chalise *et al.*, 2007; Botros Shenouda and Davidson, 2008; Wang *et al.*, 2011). In addition, "power loading" techniques have been developed for cases in which the directions of transmission have already been chosen (Payaró *et al.*, 2007; Vučić and Boche, 2009).

The principle that underlies the previous approaches to outage-based QoS problems for the downlink (Botros Shenouda and Davidson, 2008; Wang *et al.*, 2011; Payaró *et al.*, 2007; Vučić and Boche, 2009) is to seek a deterministic approximation of the outage constraint that is conservative and can be represented in a form that is convex in design variables. The conservative nature of the approximation means that any feasible point in the resulting restricted optimization problem will satisfy the original outage constraint, and the convex nature of approximations in the approaches means that a globally optimal solution to the restricted optimization problem can be efficiently found. As explained in the next section, the principles that underlie the proposed approaches are somewhat different.

1.3 Outline of the Thesis

In Chapter 2, we will describe the system model and formulate the problem of interest of this thesis. We describe CSI acquisition in TDD systems and verify the assumption of a Gaussian model for channel uncertainties in this scheme.

In Chapter 3, under the assumption of a Gaussian model for channel uncertainties, we develop a power loading technique for arbitrary beamforming directions that does not involve an approximation of the outage constraint, but, instead, employs a precise deterministic representation of the outage probability obtained as a special case of more general expressions of Al-Naffouri and Hassibi (2009). Unlike the previous approaches, the resulting optimization problem is not convex, but we develop a straightforward cyclic coordinate descent algorithm that typically produces good solutions. Indeed, in a number of scenarios our suboptimal solutions to the precise formulation of the problem provide superior performance to that of the globally

optimal solutions to the conservative approximation.

In Chapter 4 we use insight into the deterministic representation of the outage probability to construct a more computationally efficient power-loading technique for the case of nominally "zero-forcing" beamforming directions. While that technique does involve a conservative approximation, the structure of the approximation is quite different from those that have been previously applied, and numerical experience suggests that it can be significantly less conservative. Interestingly, in some important scenarios the lower level of conservatism in the approximation means that the proposed power loading algorithm with nominally zero-forcing directions yields better performance than existing conservative techniques in which the power loading and directions are designed jointly.

In Chapter 5, the different methods provided by this thesis and existing competing methods are studied in different scenarios.

In Chapter 6, the thesis is concluded with a discussion of possible future work.

Chapter 2

System Model and Problem Formulation

We consider a narrowband single-cell downlink scenario in which a base station with N_t antennas sends independent messages to K users (unicast transmission), each of which is equipped with a single antenna, as illustrated in Fig. 2.1. The base station employs linear precoding and the transmitted signal at each channel use is

$$\mathbf{x} = \sum_{k=1}^{K} \mathbf{w}_k s_k = \mathbf{W}\mathbf{s}, \tag{2.1}$$

where $\mathbf{w}_k \in \mathbb{C}^{N_t}$ is the beamforming vector for the k^{th} user and forms the k^{th} column of the precoding matrix $\mathbf{W} \in \mathbb{C}^{N_t \times K}$, and s_k is the symbol to be sent to the k^{th} user. We normalize the symbols so that they have unit energy, and since the messages are assumed to be independent we have $E\{\mathbf{s}\mathbf{s}^H\} = \mathbf{I}$. For user k, the received signal can be modeled as

$$y_k = \mathbf{h}_k^H \mathbf{x} + z_k, \tag{2.2}$$

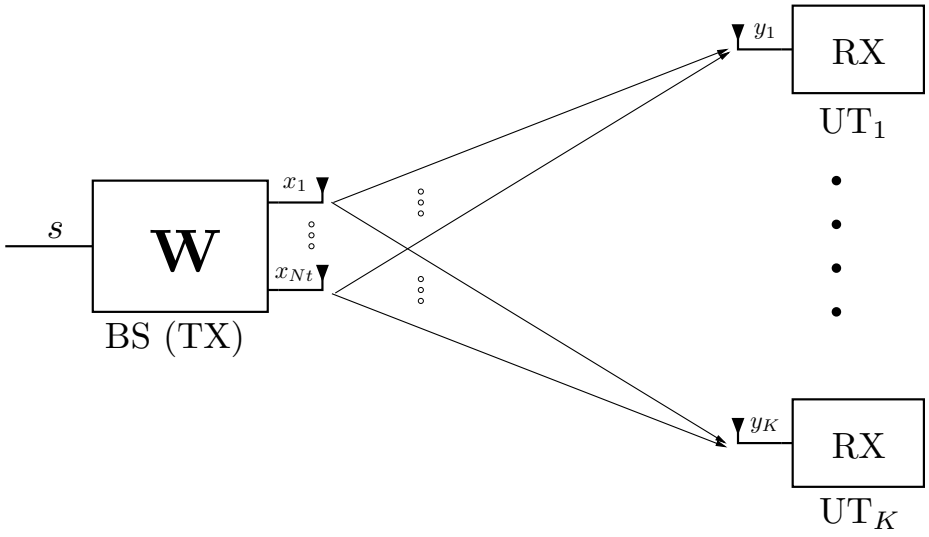

Figure 2.1: A single-cell downlink setting with N_t antennas at the base station (BS) and K users, each with a single antenna.

where $\mathbf{h}_k^H \in \mathbb{C}^{N_t}$ is the row vector of complex channel gains from the transmitting antennas to the k^{th} receiver, and z_k denotes additive noise, which is assumed to be circular complex Gaussian with zero mean and variance $\sigma_k^2 > 0$. The received signal can be rewritten as

$$y_k = \mathbf{h}_k^H \mathbf{w}_k s_k + \mathbf{h}_k^H \bar{\mathbf{W}}_k \mathbf{s} + z_k, \tag{2.3}$$

where $\bar{\mathbf{W}}_k = [\mathbf{w}_1, \ldots, \mathbf{w}_{k-1}, \mathbf{0}, \mathbf{w}_{k+1}, \ldots, \mathbf{w}_K]$. Assuming that each user terminal (UT) has perfect knowledge of the gain of intended signal, $\mathbf{h}_k^H \mathbf{w}_k$, the first term in (2.3) is the useful signal term for coherent detection of the message sent to user k, while the second term represents the interference due to the transmission to the other users and the third term is the noise.

The desire to provide service to several classes of users, and the desire to support such services with low latency requirements, has led to development of design techniques which guarantee that a certain quality of service (QoS) constraint is satisfied

for each user. In this thesis, the quality of service is specified in terms of a measure of the signal-to-interference-and-noise ratio (SINR) at user k. The appropriate measure of the SINR is dependent on the structure of the receiver and the available information at each user terminal. We will consider the case of coherent single-user detection at the users, in which the interference is treated as noise, and we will assume that each user has perfect knowledge of $\mathbf{h}_k^H \mathbf{w}_k$. In that setting, the appropriate measure of the SINR at the k^{th} user is

$$\mathsf{SINR}_k(\mathbf{W}) = \frac{|\mathbf{h}_k^H \mathbf{w}_k|^2}{\mathbf{h}_k \bar{\mathbf{W}}_k \bar{\mathbf{W}}_k^H \mathbf{h}_k + \sigma_k^2}. \tag{2.4}$$

If the BS has perfect knowledge of the channels, $\mathbf{h}_1^H, \ldots, \mathbf{h}_K^H$, then for any choice of the beamforming matrix $\mathbf{W}$, it can compute each receiver's SINR and hence it can adapt its transmission accordingly. In certain scenarios, an operator may wish to have the BS adapt its transmission so that it uses the minimum power possible, $E\{\mathbf{x}^H\mathbf{x}\} = \sum_k \|\mathbf{w}_k\|^2 = \mathrm{Tr}(\mathbf{W}\mathbf{W}^H)$, to provide selected users with a specified target SINR, or declare that it is not possible to meet that specification. That is, the BS may be required to find a set of beamformers $\{\mathbf{w}_k\}$ that solves

$$\min_{\{\mathbf{w}_k \in \mathbb{C}^{N_t}\}_{k=1}^K} \quad \mathrm{Tr}\big(\mathbf{W}\mathbf{W}^H\big) \tag{2.5a}$$

$$\text{subject to} \quad \mathsf{SINR}_k(\mathbf{W}) \geq \gamma_k, \qquad \forall k = 1, \ldots, K, \tag{2.5b}$$

or show that no such set of beamformers exists. Here, γ_k is the specified SINR for user k. This problem can be efficiently solved by transforming it into a convex second order cone program (Wiesel *et al.*, 2006) or by relaxing it to a convex semidefinite program and showing that the relaxation is tight (Bengtsson and Ottersten, 2001).

However, most wireless communication environments are dynamic, in the sense that the positions of the user terminals and/or the scattering environment change over time. In such settings, providing the BS with highly accurate estimates of the channels to the users may require a significant fraction of the available communication resources. Therefore, the BS must perform the design with imprecise knowledge of the channels.

There are a number of different strategies that can be taken in pursuing that design. The simplest strategy is to perform the design as if the estimates were exact and to hope that, over time, there is a reasonable likelihood that the performance requirements are met. A variation on that strategy is to perform the design in the "mismatched" manner, but to increase the SINR targets γ_k beyond the required level in an attempt to increase the likelihood that the mismatched design yields a solution that meets the original requirements.

An alternative strategy is to construct a model for the uncertainty in the BS's knowledge of the channel and to take that uncertainty into account in the formulation of the design problem. The model for the uncertainty is dependent on the method by which the BS obtains information about the state of the channel. In time division duplex (TDD) systems, the uplink and downlink share the same channel, but operate at different times. Therefore, if the channel changes sufficiently slowly, and appropriate RF calibration is performed (e.g., Kaltenberger *et al.*, 2010), it is possible for the base station to estimate the baseband channel gains by uplink training. For this setting, we will show in the next section that the dominant component of the CSI uncertainty can be modeled as being additive and Gaussian. In frequency division duplex (FDD) systems, each user should estimate its channel gains by downlink

training and then feed back a quantized version of those estimates to the BS on a control channel. In this setting, in addition to the estimation error at the receiver, the quantization process also introduces uncertainties, and the quantization errors typically dominate. This results in a substantially different model for the uncertainty, (e.g., Caire *et al.*, 2010). In this thesis we will focus on the TDD setting.

2.1 System Model in TDD Systems

In TDD systems, if the channel changes sufficiently slowly with respect to the length of the uplink/downlink transmission blocks, then the physical channels can be considered to be reciprocal (e.g., Smith, 2004). Although the RF chains in the base station and terminal transceivers may not be reciprocal between the uplink and the downlink, and hence the baseband equivalent channels may not necessarily be reciprocal, calibration techniques for mitigating such mismatches have proven to be effective in practice (Kaltenberger *et al.*, 2010). Therefore, when the channel changes sufficiently slowly, the channel estimates that the BS obtains in the coherent demodulation of uplink traffic, remain valid estimates for the downlink phase, and hence the BS can use those estimates to compute the precoder to be used on the downlink. These steps are illustrated in the first two blocks of Fig. 2.2.

In the proposed designs, we will assume that receivers perform coherent detection. In order to be able to do that, the k^{th} receiver needs to estimate the complex scalar $\mathbf{h}_k^H \mathbf{w}_k$. In the systems that we envision, each receiver estimates the appropriate scalar in a downlink "dedicated training" phase (Caire *et al.*, 2010). If the specification of the target SINR, γ_k, does not implicitly identify the coded modulation scheme that the BS will use to construct the sequence of symbols $\{s_k\}$, this information will be

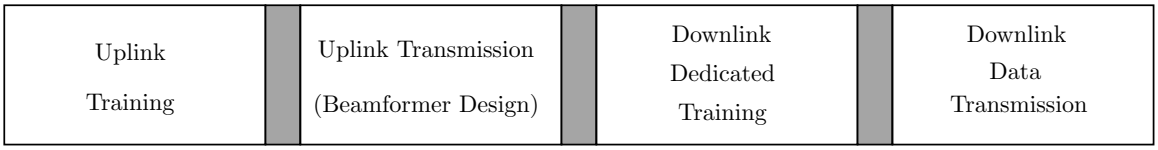

Figure 2.2: Steps of downlink transmission in TDD systems. During the uplink transmission phase, the BS would perform the beamformer design described in this thesis.

forwarded to the users on a control channel.

Once these preliminary phases have been completed, the BS transmits data to the users. The four steps involved in setting up downlink communication in a TDD system with a reciprocal channel are illustrated in Fig. 2.2. The uplink and downlink training phases will be briefly described on the following two sections, and the design problem will be formulated in Section 2.1.3. That design problem will assume that the estimation error of the downlink training phase is sufficiently small to warrant coherent detection (see, e.g., Lapidoth and Shamai, 2002). Given that it is only a complex scalar that is estimated in that phase, there are several practical schemes that enable this to be achieved with only a small amount of dedicated training, (e.g., Jindal *et al.*, 2009).

2.1.1 Uplink Training

In the uplink training phase of the systems we envision, each user transmits L_1 equal real-valued pilot symbols to the BS with power P^{UT}. We assume that each user transmits its training pilots in different time slots so that the received signal at the BS from the k^{th} user for i^{th} training symbol, $\mathbf{y}_{ki}^{\mathrm{BS}}$, can be modeled as being interference free, namely,

$$\mathbf{y}_{ki}^{\mathrm{BS}} = \sqrt{P^{\mathrm{UT}}}\mathbf{h}_k^* + \mathbf{z}_{ki}^{\mathrm{BS}}, \qquad i = 1, \ldots, L_1, \tag{2.6}$$

where $\mathbf{z}_{ki}^{\mathrm{BS}} \sim CN(\mathbf{0}, \sigma_{\mathrm{BS}}^2 \mathbf{I})$ and we have used the fact that the training symbols are assumed to be real scalar with power P^{UT}. If we concatenate the L_1 received vectors for user k into a vector $\mathbf{y}_k^{\mathrm{BS}}$, we can write

$$\mathbf{y}_k^{\mathrm{BS}} = \mathbf{T}\mathbf{h}_k^* + \mathbf{z}_k^{\mathrm{BS}}, \tag{2.7}$$

where $\mathbf{y}_k^{\mathrm{BS}} = [(\mathbf{y}_{k1}^{\mathrm{BS}})^T, \ldots, (\mathbf{y}_{kL_1}^{\mathrm{BS}})^T]^T$, $\mathbf{T} = \sqrt{P^{\mathrm{UT}}}[\mathbf{I}, ..., \mathbf{I}]^T \in \mathbb{R}^{L_1 N_t \times L_1}$ and $\mathbf{z}_k^{\mathrm{BS}} = [(\mathbf{z}_{k1}^{\mathrm{BS}})^T, \ldots, (\mathbf{z}_{kL_1}^{\mathrm{BS}})^T]^T$. The minimum mean square error (MMSE) estimate, $\hat{\mathbf{h}}_k^*$, of $\mathbf{h}_k^*$ given the observation $\mathbf{y}_k^{\mathrm{BS}}$ is obtained by (Poor, 1994)

$$\hat{\mathbf{h}}_k^* = \mathbf{C}_{\mathbf{h}_k}^T \mathbf{T}^T (\mathbf{T}\mathbf{C}_{\mathbf{h}_k}^T \mathbf{T}^T + \sigma_{\mathrm{BS}}^2 \mathbf{I})^{-1} \mathbf{y}_k^{\mathrm{BS}}, \tag{2.8}$$

where $\mathbf{C}_{\mathbf{h}_k}$ is the covariance matrix of the channel gains, $\mathbf{C}_{\mathbf{h}_k} = E\{\mathbf{h}_k \mathbf{h}_k^H\}$. The error in this estimate can be modeled as $\mathbf{h}_k^* = \hat{\mathbf{h}}_k^* + \mathbf{e}_k^*$, where $\mathbf{e}_k^*$ is independent of the estimate and is Gaussian with covariance $\mathbf{C}_k^T$

$$\mathbf{C}_k^T = \mathbf{C}_{\mathbf{h}_k^*} - \mathbf{C}_{\hat{\mathbf{h}}_k^*} = \mathbf{C}_{\mathbf{h}_k}^T - \mathbf{C}_{\mathbf{h}_k}^T \mathbf{T}^T (\mathbf{T}\mathbf{C}_{\mathbf{h}_k}^T \mathbf{T}^T + \sigma_{\mathrm{BS}}^2 \mathbf{I})^{-1} \mathbf{T}\mathbf{C}_{\mathbf{h}_k}^T. \tag{2.9}$$

Note that our aim is to model the CSI error at the BS, $\mathbf{e}_k$. According to above results, the estimation error of the channel gains is modeled as additive zero mean Gaussian random variable; i.e., $\mathbf{h}_k^H = \hat{\mathbf{h}}_k^H + \mathbf{e}_k^H$, where the covariance matrix of $\mathbf{e}_k$ is $\mathbf{C}_k$ which is given by the transpose of (2.9). The later statement is based on the fact that for a random vector $\mathbf{q}$, the covariance matrix of $\mathbf{q}$ is equivalent to transpose of the covariance matrix of $\mathbf{q}^*$; i.e., $\mathbf{C}_{\mathbf{q}} = \mathbf{C}_{\mathbf{q}^*}^T$.

For the case that the channel gains follow an i.i.d. Rayleigh fading model, i.e.,

$\mathbf{C}_{\mathbf{h}_k} = \mathbf{I}$, the covariance matrix of the error in (2.9) simplifies to

$$\mathbf{C}_k = \sigma_e^2 \mathbf{I}, \tag{2.10}$$

where $\sigma_e^2 = \frac{\sigma_{\mathrm{BS}}^2}{\sigma_{\mathrm{BS}}^2 + L_1 P^{\mathrm{UT}}}$.

2.1.2 Dedicated Training

As shown in Fig. 2.2, dedicated training is the step after beamformer design, but it is more convenient to describe the dedicated training phase first. Once the BS has computed the beamforming matrix $\mathbf{W}$, coherent detection is enabled by additional downlink training transmitted along each beamforming vector. For coherent detection at the k^{th} user, that terminal needs a high quality estimate of $\mathbf{h}_k^H \mathbf{w}_k$. So at different time slots the BS transmits L_2 pilot symbols with power P^{BS} in the direction of $\mathbf{w}_k$. The observed signal at the k^{th} user in response to the i^{th} pilot symbol for that user can be written as

$$y_{ki}^{\mathrm{UT}} = \frac{\sqrt{P^{\mathrm{BS}}}}{\|\mathbf{w}_k\|} \mathbf{h}_k^H \mathbf{w}_k + z_{ki}^{\mathrm{UT}}, \qquad i = 1, \ldots, L_2, \tag{2.11}$$

where $z_{ki}^{\mathrm{UT}} \sim CN(0, \sigma_k^2)$. By concatenating those observed signals in to a vector $\mathbf{y}_k^{\mathrm{UT}}$, we can write

$$\mathbf{y}_k^{\mathrm{UT}} = \mathbf{t}(\mathbf{h}_k^H \mathbf{w}_k) + \mathbf{z}_k^{\mathrm{UT}}, \tag{2.12}$$

where $\mathbf{y}_k^{\mathrm{UT}} = [y_{k1}^{\mathrm{UT}}, \ldots, y_{kL_2}^{\mathrm{UT}}]^T$, $\mathbf{t} = \frac{\sqrt{P^{\mathrm{BS}}}}{\|\mathbf{w}_k\|}\mathbf{1} \in \mathbb{R}^{L_2}$ and $\mathbf{z}_k^{\mathrm{UT}} = [z_{k1}^{\mathrm{UT}}, \ldots, z_{kL_2}^{\mathrm{UT}}]^T$. By using an MMSE estimator at each user, the receiver's estimate of $\mathbf{h}_k^H \mathbf{w}_k$, which we

denote by $\widehat{\mathbf{h}_k^H \mathbf{w}_k}$, is found as follows

$$\widehat{\mathbf{h}_k^H \mathbf{w}_k} = c\mathbf{t}^T(\mathbf{t}c\mathbf{t}^T + \sigma_k^2\mathbf{I})^{-1}\mathbf{y}_k^{\mathrm{UT}}, \tag{2.13}$$

where c is the variance of $\mathbf{h}_k^H \mathbf{w}_k$. In terms of the estimate $\widehat{\mathbf{h}_k^H \mathbf{w}_k}$ and estimation error $\tilde{e}_k$, $\mathbf{h}_k^H \mathbf{w}_k$ can be written as

$$\widehat{\mathbf{h}_k^H \mathbf{w}_k} = \mathbf{h}_k^H \mathbf{w}_k + \tilde{e}_k, \tag{2.14}$$

where $\tilde{e}_k$ is independent of the estimate and is Gaussian with variance

$$\sigma_{\tilde{e}_k}^2 = \frac{c\sigma_k^2}{\sigma_k^2 + cL_2 \frac{P^{\mathrm{BS}}}{\|\mathbf{w}_k\|^2}}. \tag{2.15}$$

Although the format of error in dedicated training phase is similar to the format of error in uplink training phase, we can assume that dedicated training phase is performed perfectly. There are some reasons that support this assumption. In dedicated training phase user seeks to estimate just a scalar rather than a vector in uplink training phase. In addition, the BS typically has access to greater energy reserves than small mobile devices (Salim *et al.*, 2012). So if the BS transmits sufficient pilots in dedicated training phase, we can neglect the effect of the error in this phase. By neglecting that error, we assume that k^{th} user knows $\mathbf{h}_k^H \mathbf{w}_k$ perfectly, which means each user has perfect knowledge about the gain of the intended data, so the SINR metric in (2.4) is indeed the metric that demonstrates system performance; (see also Lapidoth and Shamai, 2002).

2.1.3 Beamformer Design Based on Performance Metric

As illustrated in Fig. 2.2, once the base station has estimated the uplink channels, and while it is receiving data on the uplink, it designs the beamforming vectors, $\mathbf{w}_k$. It does so by using what CSI it has to estimate a performance metric for the receivers and then seeking beamformers that optimize that metric. As we have discussed earlier, the problem of interest in this thesis is to minimize the transmission power at the BS that is required to ensure that an SINR-based QoS constraint is met.

One approach to deal with the uncertainty in the BS knowledge of the CSI is to assume a bounded model for the uncertainty and to design a transmitter that satisfies the QoS requirements even for the worst case of the uncertainties admitted by the model; (e.g., Botros Shenouda and Davidson, 2007; Zheng *et al.*, 2008; Vucic and Boche, 2009; Botros Shenouda and Davidson, 2009). The general problem formulation of bounded uncertainty model for problem of interest in this thesis is

$$\min_{\{\mathbf{w}_k \in \mathbb{C}^{N_t}\}_{k=1}^{K}} \quad \mathrm{Tr}\big(\mathbf{W}\mathbf{W}^H\big) \tag{2.16a}$$

$$\text{subject to} \quad \mathsf{SINR}_k(\mathbf{W}) \geq \gamma_k, \qquad \forall k, \forall \mathbf{h}_k \in \mathcal{H}_k, \tag{2.16b}$$

where $\mathcal{H}_k$ denotes the given an uncertainty set for the channel to user k. Although this approach sounds reasonable, using the beamforming matrix that is optimal in the worse-case does not necessarily lead to good performance in typical cases. Furthermore, in the TDD case that we are interested in, the natural uncertainty model is not bounded, and hence there is a fundamental mismatch between the bounded uncertainty model and the nature of the uncertainty as it arises in practice.

Another approach to dealing with uncertainty that is less prone to these mismatches is to model the uncertainty stochastically and to seek to satisfy the QoS constraint with a given probability. In the following paragraphs, we will explore that approach for both the case of precoder design and the case of power loading, where the beamformer directions are predefined.

Chance-constrained Robust Precoding

For given SINR targets γ_k, the quality of service constraint in this case is that the probability that $\mathsf{SINR}_k(\mathbf{W}) \geq \gamma_k$ should be greater than $1-\epsilon_k$, for a pre-specified parameter ϵ_k. Therefore, given the uncertainty model $\mathbf{h}_k = \hat{\mathbf{h}}_k + \mathbf{e}_k$ and a distribution for $\mathbf{e}_k$, the problem of interest can be written as

$$\min_{\{\mathbf{w}_k \in \mathbb{C}^{N_t}\}_{k=1}^{K}} \quad \mathrm{Tr}\big(\mathbf{W}\mathbf{W}^H\big) \tag{2.17a}$$

$$\text{subject to} \quad \mathrm{Pr}_{\mathbf{e}_k}\big(\mathsf{SINR}_k(\mathbf{W}) \geq \gamma_k\big) \geq 1-\epsilon_k, \qquad \forall k, \tag{2.17b}$$

where the SINR at user k is defined as in (2.4). The presence of the chance constraints in (2.17b) makes the problem difficult to tackle directly, especially because the SINR in (2.4) is the ratio of a quadratic functions of the design variables. One approach is to apply a conservative transformation to the SINR constraint in (2.17b) to convert the problem in (2.17) into a chance-constrained second-order cone program (SOCP) (Botros Shenouda and Davidson, 2008). By applying various conservative approximations of chance-constrained SOCPs, efficiently-solvable deterministic convex optimization problems are obtained (some are SOCPs, others are semidefinite programs, SDPs). The conservative nature of the approximations means that when

these convex problems are feasible, the solution is guaranteed to satisfy the chance constraints in (2.17b). The related approach of Wang *et al.* (2011) first applies a semidefinite relaxation to the problem in (2.17), which yields a semidefinite program (SDP) with chance constraints on quadratic functions of a vector of variables. These chance constraints are then conservatively approximated by deterministic convex constraints leading to an SDP formulation. One of the SDP problem formulations obtained using this approach for a zero mean i.i.d. Gaussian uncertainty model involves optimizing over $\mathbf{U}_k = \mathbf{w_k}\mathbf{w}_k^H$ where $\mathbf{U}_k$ is a Hermitian matrix, $\mathbf{U}_k \in \mathbb{H}^{N_t \times N_t}$, and conservatively approximating the chance constraint by a linear matrix inequality (Wang *et al.*, 2011). The resulting SDP is

$$\min_{\{\mathbf{U}_k \in \mathbb{H}^{N_t \times N_t}\}, \{t_k \geq 0\}} \quad \sum_k \mathrm{Tr}\big(\mathbf{U}_k\big) \tag{2.18a}$$

$$\text{subject to} \quad \begin{bmatrix} \mathbf{Q}_k + t_k \mathbf{I} & \mathbf{r}_k \\ \mathbf{r}_k^H & v_k - t_k {d_k}^2 \end{bmatrix} \succeq \mathbf{0}, \qquad \forall k, \tag{2.18b}$$

where $\mathbf{Q}_k = \mathbf{C}_k^{1/2}\Big(\frac{1}{\gamma_k}\mathbf{U}_k - \sum_{j \neq k}\mathbf{U}_j\Big)\mathbf{C}_k^{1/2}$, $\mathbf{r}_k = \mathbf{C}_k^{1/2}\Big(\frac{1}{\gamma_k}\mathbf{U}_k - \sum_{j \neq k}\mathbf{U}_j\Big)\hat{\mathbf{h}}_k$, $v_k = \hat{\mathbf{h}}_k\Big(\frac{1}{\gamma_k}\mathbf{U}_k - \sum_{j \neq k}\mathbf{U}_j\Big)\hat{\mathbf{h}}_k - \sigma_k^2$ and $d_k = \sqrt{{\phi^{-1}}_{X^2_{2N_t}}(1-\epsilon_k)/2}$, where ${\phi^{-1}}_{X^2_{2N_t}}(\cdot)$ is the inverse cumulative distribution function of central Chi-square random variable with $2N_t$ degrees of freedom. The solution to this problem is guaranteed to satisfy the chance constraints in (2.17b) whenever each of the solution matrices in (2.18) has rank one. Numerical experiments by Wang *et al.* (2011) suggest that this is almost always the case.

Chance-constrained Robust Power Loading

In robust precoding the directions of transmission, $\breve{\mathbf{w}}_k = \mathbf{w}_k/||\mathbf{w}_k||_2$, and the power allocated to each direction, $\breve{p}_k = ||\mathbf{w}_k||_2^2$, are found jointly. A potentially simpler approach is to choose the directions $\breve{\mathbf{w}}_k$ based on the transmitters' channel estimates $\hat{\mathbf{h}}_k$ and then to seek solutions to the problem in (2.17) over the K powers, $\breve{p}_k$. It is often more convenient to remove the restriction that the directions be specified in a normalized form, and simply pre-specify vectors. We will pre-specify the directions as not necessarily normalized vectors $\mathbf{b}_k$ and seek a power allocation $\{p_k\}$ for these vectors so that $\mathbf{w}_k = \sqrt{p_k}\,\mathbf{b}_k$. In that case, the total power transmitted is $\sum_{k=1}^{K} p_k \|\mathbf{b}_k\|_2^2$. If we define $\mathbf{B} = [\mathbf{b}_1, \mathbf{b}_2, ..., \mathbf{b}_K]$ and $\mathbf{P} = \mathrm{Diag}(p_1, p_2, ..., p_K)$, the robust power loading problem can be written as

$$\min_{\{p_k \geq 0\}} \ \mathrm{Tr}\big(\mathbf{B}\mathbf{P}\mathbf{B}^H\big) \tag{2.19a}$$

$$\text{s.t. } \Pr_{\mathbf{e}_k}\Big(\frac{|(\hat{\mathbf{h}}_k^H + \mathbf{e}_k^H)\mathbf{b}_k|^2 p_k}{(\hat{\mathbf{h}}_k^H + \mathbf{e}_k^H)\bar{\mathbf{B}}_k\mathbf{P}\bar{\mathbf{B}}_k^H(\hat{\mathbf{h}}_k + \mathbf{e}_k) + \sigma_k^2} \geq \gamma_k\Big) \geq 1 - \epsilon_k, \qquad \forall k, \tag{2.19b}$$

where $\bar{\mathbf{B}}_k = [\mathbf{b}_1, ..., \mathbf{b}_{k-1}, \mathbf{0}, \mathbf{b}_{k+1}, ..., \mathbf{b}_K]$. A common choice for the precoding matrix $\mathbf{B}$ is the regularized channel inversion precoder for the estimated channel (Peel *et al.*, 2005): Given matrix of channel estimates $\hat{\mathbf{H}} = [\hat{\mathbf{h}}_1, \hat{\mathbf{h}}_2, ..., \hat{\mathbf{h}}_K]^H$ and a non-negative real number α,

$$\mathbf{B}_{\mathrm{RCI}} = \hat{\mathbf{H}}^H\big(\hat{\mathbf{H}}\hat{\mathbf{H}}^H + \alpha\mathbf{I}_K\big)^{-1}. \tag{2.20}$$

In the special case when $\alpha = 0$, the nominal zero-forcing precoder is obtained where

$$\mathbf{B}_{\mathrm{ZF}} = \hat{\mathbf{H}}^H\big(\hat{\mathbf{H}}\hat{\mathbf{H}}^H\big)^{-1}. \tag{2.21}$$

In the development of approaches to solve the problem in (2.19), it can be helpful to write down the chance constraints in (2.19b) in the form of chance constraints on a quadratic function of a standard complex Gaussian random variable, $\boldsymbol{\delta}_k \sim CN(\mathbf{0}, \mathbf{I})$, namely,

$$\Pr_{\boldsymbol{\delta}_k}\big(\boldsymbol{\delta}_k^H \mathbf{Q}_k \boldsymbol{\delta}_k + 2\,\mathrm{Re}(\boldsymbol{\delta}_k^H \mathbf{r}_k) + v_k \geq 0\big) \geq 1 - \epsilon_k, \tag{2.22}$$

where $\mathbf{Q}_k = {\mathbf{C}_k}^{1/2}\big(\frac{p_k}{\gamma_k}\mathbf{b}_k\mathbf{b}_k^H - \bar{\mathbf{B}}_k\mathbf{P}\bar{\mathbf{B}}_k^H\big){\mathbf{C}_k}^{1/2}$, $\mathbf{r}_k = {\mathbf{C}_k}^{1/2}\big(\frac{p_k}{\gamma_k}\mathbf{b}_k\mathbf{b}_k^H - \bar{\mathbf{B}}_k\mathbf{P}\bar{\mathbf{B}}_k^H\big)\hat{\mathbf{h}}_k$ and $v_k = \hat{\mathbf{h}}_k^H\big(\frac{p_k}{\gamma_k}\mathbf{b}_k\mathbf{b}_k^H - \bar{\mathbf{B}}_k\mathbf{P}\bar{\mathbf{B}}_k^H\big)\hat{\mathbf{h}}_k - \sigma_k^2$. By writing the chance constraints in this form, a number of existing conservative deterministic approximations to the chance constrain can be applied in a straightforward way (see Wang *et al.*, 2011). For example, given $\mathbf{B}$, the solution to the following SDP yields powers $\{p_k\}$ that satisfy the constraints in (2.19),

$$\min_{\{p_k\geq 0\},\,\{t_k\geq 0\}} \quad \mathrm{Tr}\big(\mathbf{B}\mathbf{P}\mathbf{B}^H\big) \tag{2.23a}$$

$$\text{subject to} \quad \begin{bmatrix} \mathbf{Q}_k + t_k\mathbf{I} & \mathbf{r}_k \\ \mathbf{r}_k^H & v_k - t_k {d_k}^2 \end{bmatrix} \succeq \mathbf{0}, \qquad \forall k, \tag{2.23b}$$

where $d_k = \sqrt{{\phi^{-1}}_{X^2_{2N_t}}(1-\epsilon_k)/2}$. That said, since (2.23) is based on a conservative approximation, the absence of a solution to (2.23) does not necessarily mean that there are no powers that satisfy (2.19).

The goal of this thesis is to propose robust power loading algorithms that reduce conservatism and may reduce the computational cost.

2.1.4 Data Transmission

The last step in the operation of the downlink illustrated in Fig. 2.2 is data transmission. The BS transmits independent messages to K users using linear beamformers which are obtained in beamformer design phase. As discussed earlier, the transmitted signal has the form in (2.1) and the received signal has the form in (2.3) or (2.4). Assuming that each receiver employs coherent detection, the conventional SINR in (2.4) is the performance metric.

2.2 FDD Systems

Although the focus of this thesis is on TDD systems, for the completeness of the context, we now briefly describe the operation of FDD systems. In an FDD system, since the uplink and downlink use different frequency bands, we cannot obtain accurate information about the downlink channel by sending pilots on the uplink channel. In this setting, downlink transmission typically consists of the five steps illustrated in Fig. 2.3. First, the BS sends training symbols to the users and each user estimates their channel. In simple FDD systems, each user then sends back their estimate on a control channel. (In some more sophisticated systems, users may decide to censor themselves if their received SINR is not sufficient to support the service that they require.) As articulated by Caire *et al.* (2010), there are many advantages of feeding back, digitally, a quantized version of the channel estimate. Typically, we assume that the BS receives this quantized version perfectly. In this setting, we have two sources of error in the base station's estimate of the CSI, the estimation error of channel gains in the training phase and the quantization error incurred in feedback

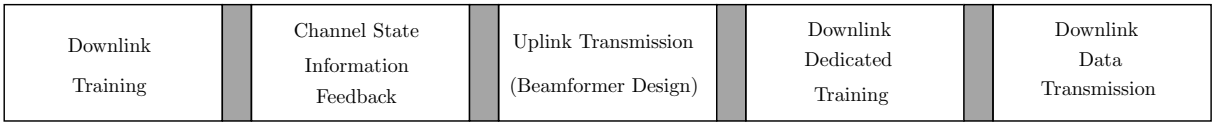

Figure 2.3: Steps of downlink transmission in FDD systems.

phase. In practice, the second source of error tends to dominate and, depending on the quantization scheme, the quantization error can be quite difficult to model analytically. This makes it difficult to faithfully approximate the chance constraints with deterministic expressions, and that, in turn restricts the development of effective algorithm. For that reason we will focus on TDD systems in this thesis.

Once the BS has an estimate of the channels, it can design the precoder, and then perform the dedicated training and data transmission steps that are similar to the TDD case, which was illustrated in Fig. 2.2.

Chapter 3

A Non-conservative Approach to Chance-constrained Robust Power Loading

In this chapter we develop a cyclic coordinate descent algorithm for finding good solutions to the problem of minimizing the transmitter power required for each user terminal to obtain its specified SINR with a specified probability under a zero mean Gaussian model for the channel uncertainty; that is, problem (2.19) in the case that $\mathbf{e}_k \sim \mathcal{CN}(\mathbf{0}, \mathbf{C}_k)$. Unlike previous approaches, such as those that led to (2.23), we do not seek a conservative deterministic approximation of the chance constraint in (2.22), $\Pr_{\boldsymbol{\delta}_k}\big(\boldsymbol{\delta}_k^H \mathbf{Q}_k \boldsymbol{\delta}_k + 2\,\mathrm{Re}(\boldsymbol{\delta}_k^H \mathbf{r}_k) + v_k \geq 0\big) \geq 1 - \epsilon_k$, that results in a tractable convex, but conservative, formulation. Instead, we employ a closed-form expression for the probability that the SINR constraint is satisfied. This expression is derived from a more general expression obtained by Al-Naffouri and Hassibi (2009).

3.1 A Closed-form Expression for the CDF of a Quadratic Function of a Gaussian Random Vector

In this section we present a result of Al-Naffouri and Hassibi (2009) that provides a closed-form expression for the cumulative distribution function (CDF) of a quadratic function of a standard circular complex Gaussian random vector. This result is a key step in the development of the proposed design algorithm.

Lemma 1 (Al-Naffouri and Hassibi (2009))**.** *Given a deterministic Hermitian symmetric matrix* $\mathbf{Q}$ *and a deterministic vector* $\mathbf{a}$*, for the standard circular complex Gaussian random vector* $\mathbf{x} \sim CN(\mathbf{0}, \mathbf{I})$*, the CDF of* $\|\mathbf{x}-\mathbf{a}\|_{\mathbf{Q}}^2 = (\mathbf{x}-\mathbf{a})^H\mathbf{Q}(\mathbf{x}-\mathbf{a})$*,* $\Pr\big(\|\mathbf{x}-\mathbf{a}\|_{\mathbf{Q}}^2 \leq \tau\big)$*, is*

$$\frac{1}{2\pi}\int_{-\infty}^{\infty} \frac{e^{\tau(i\omega+\beta)}}{i\omega+\beta} \frac{e^{-c}}{\det(\mathbf{I}+(i\omega+\beta)\mathbf{Q})} d\omega, \tag{3.1}$$

for some $\beta > 0$ *such that* $\mathbf{I}+\beta\mathbf{Q}$ *is positive definite. If we let* $\mathbf{Q} = \mathbf{V}\mathbf{\Lambda}\mathbf{V}^H$ *denote the eigen-decomposition of* $\mathbf{Q}$*, with* λ_m *denoting the eigenvalues arranged in descending order* $\big(\mathbf{\Lambda} = \mathrm{Diag}(\lambda_1, \lambda_2, \dots)\big)$*, and if we define* $\tilde{\mathbf{a}} = \mathbf{V}^H\mathbf{a}$*, the constant* c *can be written as* $c = \sum_{m=1}^{M} \frac{|\tilde{a}_m|^2(i\omega+\beta)\lambda_m}{1+(i\omega+\beta)\lambda_m}$*.*

The second statement in Lemma 1 is slightly more general than that in (Al-Naffouri and Hassibi, 2009) because it does not require $\mathbf{Q}$ to be invertible. In the application in this thesis, that is important when there are fewer active users than transmitting antennas. As there are some weaknesses in the proof of Lemma 1 provided by Al-Naffouri and Hassibi (2009), a complete proof is provided in Appendix A.

In order to employ Lemma 1 in our context, we reformat the chance constraint in (2.22), which is

$$\Pr\big(\boldsymbol{\delta}_k^H \mathbf{Q}_k \boldsymbol{\delta}_k + 2\,\mathrm{Re}(\boldsymbol{\delta}_k^H \mathbf{r}_k) + v_k \geq 0\big) \geq 1 - \epsilon_k, \tag{3.2}$$

into a format that is compatible to Lemma 1. The resulting expression is

$$\Pr\big(\|\boldsymbol{\delta}_k - \mathbf{a}_k\|^2_{(-\mathbf{Q}_k)} \leq \tau_k\big) \geq 1 - \epsilon_k, \tag{3.3}$$

where $\mathbf{a}_k = -{\mathbf{C}_k}^{-1/2}\hat{\mathbf{h}}_k$ and $\tau_k = v_k - \mathbf{a}_k^H \mathbf{Q}_k \mathbf{a}_k$. To verify this expression, we observe that

$$\begin{aligned}
\|\boldsymbol{\delta}_k - \mathbf{a}_k\|^2_{(-\mathbf{Q}_k)} \leq \tau_k &\equiv (\boldsymbol{\delta}_k - \mathbf{a}_k)^H(-\mathbf{Q}_k)(\boldsymbol{\delta}_k - \mathbf{a}_k) \leq \tau_k \\
&\equiv -\boldsymbol{\delta}_k^H \mathbf{Q}_k \boldsymbol{\delta}_k + 2\,\mathrm{Re}(\boldsymbol{\delta}_k^H \mathbf{Q}_k \mathbf{a}_k) - \mathbf{a}_k^H \mathbf{Q}_k \mathbf{a}_k \leq \tau_k \\
&\equiv \boldsymbol{\delta}_k^H \mathbf{Q}_k \boldsymbol{\delta}_k - 2\,\mathrm{Re}(\boldsymbol{\delta}_k^H \mathbf{Q}_k \mathbf{a}_k) + \mathbf{a}_k^H \mathbf{Q}_k \mathbf{a}_k + \tau_k \geq 0.
\end{aligned} \tag{3.4}$$

According to the definitions of $\mathbf{Q}_k$, $\mathbf{r}_k$ and v_k in (3.2) (i.e., $\mathbf{Q}_k = {\mathbf{C}_k}^{1/2}\big(\frac{p_k}{\gamma_k}\mathbf{b}_k\mathbf{b}_k^H - \bar{\mathbf{B}}_k\mathbf{P}\bar{\mathbf{B}}_k^H\big){\mathbf{C}_k}^{1/2}$, $\mathbf{r}_k = {\mathbf{C}_k}^{1/2}\big(\frac{p_k}{\gamma_k}\mathbf{b}_k\mathbf{b}_k^H - \bar{\mathbf{B}}_k\mathbf{P}\bar{\mathbf{B}}_k^H\big)\hat{\mathbf{h}}_k$ and $v_k = \hat{\mathbf{h}}_k^H\big(\frac{p_k}{\gamma_k}\mathbf{b}_k\mathbf{b}_k^H - \bar{\mathbf{B}}_k\mathbf{P}\bar{\mathbf{B}}_k^H\big)\hat{\mathbf{h}}_k - \sigma_k^2$), it can be seen that if we define $\mathbf{a}_k = -{\mathbf{C}_k}^{-1/2}\hat{\mathbf{h}}_k$ and $\tau_k = v_k - \mathbf{a}_k^H\mathbf{Q}_k\mathbf{a}_k = -\sigma_k^2$, (3.4) is equivalent to the argument of probability function in (3.2).

3.2 Coordinate Descent Algorithm

By using the results of Section 3.1, we can rewrite the optimization problem of robust power loading in a form that is no longer chance-constrained, but is deterministically

constrained. The resulting problem is

$$\min_{\{p_k \geq 0\}} \quad \mathrm{Tr}\big(\mathbf{B}\mathbf{P}\mathbf{B}^H\big) \tag{3.5a}$$

$$\text{s.t.} \quad \frac{1}{2\pi}\int_{-\infty}^{\infty} \frac{e^{\tau_k(i\omega+\beta)}}{i\omega+\beta}\frac{e^{-c_k}}{\det(\mathbf{I}-(i\omega+\beta)\mathbf{Q}_k)}d\omega \geq 1-\epsilon_k, \qquad \forall k, \tag{3.5b}$$

where $\mathbf{Q}_k$ and τ_k are defined analogous to the definition in (3.4) and c_k has a format analogous to the format of c in Lemma 1. This deterministic problem is not convex, but we will now develop a simple algorithm that works well in practice.

The proposed algorithm starts with a diagonal power allocation matrix $\mathbf{P}^{(0)}$ for which all the integral constraints in (3.5b) are satisfied. (We will discuss techniques for finding such a $\mathbf{P}^{(0)}$ below.) The algorithm then seeks a power allocation of lower cost that remains feasible via cyclic coordinate descent (e.g., Bertsekas, 1999, Sections 2–7). We will describe the steps in each cycle in the natural order, but the principles apply to any ordering of $\{p_k\}$.

At the k^{th} step of the i^{th} cycle of the coordinate descent algorithm, we seek to reduce the value of p_k given fixed values for the other powers. For $j = 1, \ldots, k-1$, those power are the ones calculated in the current cycle, i.e., $p_j = p_j^{(i)}$, whereas for $j = k+1, \ldots, K$, those powers are the ones calculated in the previous cycle, i.e., $p_j = p_j^{(i-1)}$. Since the integral in (3.5b) is equivalent to $\Pr\big(\mathsf{SINR}_k \geq \gamma_k\big)$, we can interpret the behaviour of the integral by looking at the definition of the SINR. For fixed-direction beamformers, we can rewrite the SINR in (2.4) in terms of the powers as

$$\mathrm{SINR}_k = \frac{|\mathbf{h}_k^H\mathbf{b}_k|^2 p_k}{\sum_{j\neq k}|\mathbf{h}_k^H\mathbf{b}_j|^2 p_j + \sigma_k^2}. \tag{3.6}$$

An important observation from the expression in (3.6) is that p_k appears only in the

numerator. Hence, a reduction in p_k results in a reduction in SINR_k. On the other hand, all $p_j, j \neq k$, appear only in the dominator so a reduction in p_j, $j \neq k$, results in an increase in SINR_k. Using these two facts, it is guaranteed that when performing the descent step on p_k we need only consider the integral constraint which is equivalent to the constraint on SINR_k. The constraints on SINR_j, $\forall j \neq k$, are guaranteed to remain satisfied.

The arguments in the previous paragraph show that we can reduce the value of p_k, and hence the total transmitted power, by reducing the extent to which the constraint on SINR_k is "over satisfied". To put that into practice in a cyclic coordinate algorithm, at the k^{th} step of the i^{th} cycle we choose a value for $\Delta_k^{(i)} \leq \Delta_k^{(i-1)}$ and perform bisection search on the interval $[0, p_k^{(i-1)}]$ for a value of p_k such that the probability that $\mathsf{SINR}_k \geq \gamma_k$ lies in the interval $[1-\epsilon_k, 1-\epsilon_k+\Delta_k^{(i)}]$. The probability is calculated using the integral expression in (3.5b) with c_k, τ_k, $\mathbf{Q}_k$ calculated using $p_1^{(i)}, \ldots, p_{k-1}^{(i)}, p_{k+1}^{(i-1)}, \ldots, p_K^{(i-1)}$ and the midpoint for the current interval in the bisection search for $p_k^{(i)}$. The algorithm is terminated once we find a power allocation $\mathbf{P}^{(i)}$ such that for each k the probability that $\mathsf{SINR}_k \geq \gamma_k$ lies in the interval $[1-\epsilon_k, 1-\epsilon_k+\Delta_k^{\min}]$, where $\Delta_k^{\min}$ is a pre-specified bound, or a pre-specified number of cycles is reached. A feature of this algorithm is that at each step in each cycle the power allocation $\{p_1^{(i)}, p_2^{(i)}, \ldots, p_k^{(i)}, p_{k+1}^{(i-1)}, \ldots, p_K^{(i-1)}\}$ is feasible and hence whenever the algorithm is terminated, the current power allocation will satisfy the specified QoS constraints of the original problem. Furthermore, at each step in each cycle, the objective value decreases, or remains the same. The later case occurs when the termination criteria is satisfied prior to performing the current coordinate descent step and therefore the algorithm will go on to the next step without any changes in

the power allocation.

The parameter $\Delta_k^{\min}$ is one of the parameter of the algorithm that enables us to make trade offs between the performance and the complexity of the algorithm. A smaller value for $\Delta_k^{\min}$ results in less conservative solutions that are achieved using less transmitted power. However, a smaller value for $\Delta_k^{\min}$ also results in smaller interval for the stopping criteria, which would typically lead to a larger number of cycles. Hence, for smaller $\Delta_k^{\min}$ the complexity of the algorithm is increased. The other parameter that effects on the complexity of the algorithm is $\Delta_k^{(i)}$. A smaller value for $\Delta_k^{(i)}$ results in more bisections steps in the k^{th} step of the i^{th} cycle, and that increases the computational cost of each cycle, but it also produces a better power allocation at the end of each cycle. That may help to reduce the number of cycles; hence, the nett effect of $\Delta_k^{(i)}$ on the complexity is not explicit. One useful strategy for defining $\Delta_k^{(i)}$ is to pick larger values for early cycles and then choose smaller values as the cycle index increases; i.e., $\Delta_k^{(i-1)} \geq \Delta_k^{(i)}$. Arguably, the simplest strategy is to define $\Delta_k^{(i)}$ to be a constant value equal to $\Delta_k^{\min}$ for all cycles; i.e., $\Delta_k^{(i)} = \Delta_k^{\min}$, and that is what we will do in the experiments in Chapter 5.

To complete the description of the algorithm, we need to establish a method to determine a feasible starting point. As the feasible set in (3.5) is not necessarily convex, determining whether or not an instance of the problem in (3.5) is feasible can be computationally demanding task. Instead, we simply seek an approach that often finds feasible points for reasonable instances of the problem. The proposed approach involves selecting an initial diagonal power allocation matrix and evaluating each of the integral in (3.5b). If that power allocation is not feasible, the allocation is iteratively doubled until a feasible allocation is found or the power become unreasonably

large. In the latter case a new initial power allocation can be selected and the search for a feasible allocation repeated, or the algorithm reports that no feasible point was found. In our implementation we have found that choosing the initial power allocation to be the power allocation that would be chosen if the channel estimates $\hat{\mathbf{h}}_k^H$ were exact (perfect CSI) and if each SINR_k were set to be equal to its lower bound typically leads to a feasible starting point for the main algorithm after a small number of doubling iterations. By rearranging the terms in the SINR expression, one can obtain the initial power allocation by solving a set of linear equations, as we will now show.

By assuming the perfect channel state information, which means $\mathbf{e}_k = \mathbf{0}, \forall k$, the original probabilistic constraint, $\Pr\big(\boldsymbol{\delta}_k^H \mathbf{Q}_k \boldsymbol{\delta}_k + 2\,\mathrm{Re}(\boldsymbol{\delta}_k^H \mathbf{r}_k) + v_k \geq 0\big) \geq 1 - \epsilon_k$, is simplified to $v_k \geq 0$, which is a deterministic constraint. According to definition of v_k in (2.22), we have $v_k = \hat{\mathbf{h}}_k^H \big(\frac{p_k}{\gamma_k}\mathbf{b}_k\mathbf{b}_k^H - \bar{\mathbf{B}}_k \mathbf{P} \bar{\mathbf{B}}_k^H\big)\hat{\mathbf{h}}_k - \sigma_k^2$. We can rewrite these inequalities in a matrix format as:

$$\begin{pmatrix} n_1^2 & -m_{21}^2 & \dots & -m_{K1}^2 \\ -m_{12}^2 & n_2^2 & \dots & -m_{K2}^2 \\ \vdots & \vdots & \ddots & \vdots \\ -m_{1K}^2 & -m_{2K}^2 & \dots & n_K^2 \end{pmatrix} \begin{pmatrix} p_1 \\ p_2 \\ \vdots \\ p_K \end{pmatrix} \geq \begin{pmatrix} \sigma_1^2 \\ \sigma_2^2 \\ \vdots \\ \sigma_K^2 \end{pmatrix}, \tag{3.7}$$

where $m_{ik} = |\hat{\mathbf{h}}_k^H \mathbf{b}_i|$ and $n_k = \frac{1}{\sqrt{\gamma_k}} |\hat{\mathbf{h}}_k^H \mathbf{b}_k|$. The desired powers can then be obtained by solving the set of linear equations that arise in the case of equality in (3.7).

The proposed robust power allocation algorithm is summarized in Algorithm 1. As the problem in (3.5) is not convex, the proposed algorithm is not guaranteed to find the globally optimal solution. Indeed, it is not even guaranteed to find a feasible

Algorithm 1

Start with a feasible diagonal power allocation matrix $\mathbf{P} = \mathbf{P}^{(0)}$
for $i = 1 \rightarrow iteration_{max}$ **do**
    For all k, choose $\Delta_k^{(i)}$ such that $\Delta_k^{(i)} \leq \Delta_k^{(i-1)}$
    for $k = 1 \rightarrow K$ **do**
        Find $p_k = p_k^{(i)}$ by using bisection search such that:
        $\{p_k^{(i)} \in [0, p_k^{(i-1)}] \mid 1 - \epsilon_k \leq \frac{1}{2\pi} \int_{-\infty}^{\infty} \frac{e^{\tau_k (i\omega+\beta)}}{i\omega+\beta} \frac{e^{-c_k}}{\det(\mathbf{I} - (i\omega+\beta)\mathbf{Q}_k)} d\omega \leq 1 - \epsilon_k + \Delta_k^{(i)}\}$
    end for
    if $\forall k;\ 1 - \epsilon_k \leq \frac{1}{2\pi} \int_{-\infty}^{\infty} \frac{e^{\tau_k (i\omega+\beta)}}{i\omega+\beta} \frac{e^{-c_k}}{\det(\mathbf{I} - (i\omega+\beta)\mathbf{Q}_k)} d\omega \leq 1 - \epsilon_k + \Delta_k^{\min}$ **then**
        STOP
    end if
end for

point when one exists. However, we will demonstrate in Chapter 5 that by tackling the problem directly, without a conservative approximation, the proposed approach often provides better performance than the existing conservative approaches. Having said that, the repeated requirement to compute an integral of the form in (3.5b) imposes a significant computational burden. (The SDPs that must be solved in the existing conservative approaches, such as those in (2.18), also impose a significant computational burden.) To address this issue, in the following sections we will develop customized variants of the algorithm for the case of the zero-forcing directions; i.e., $\mathbf{B} = \mathbf{B}_{\text{ZF}} = \hat{\mathbf{H}}^H \big(\hat{\mathbf{H}}\hat{\mathbf{H}}^H\big)^{-1}$.

Chapter 4

Efficient Conservative Algorithms for the Zero-Forcing Case

In Chapter 3, we proposed a coordinate descent algorithm for any fixed-direction beamforming. That algorithm involves repeated calculation of integrals in the form of (3.1). Since calculating of these integrals is computationally expensive, in this chapter we seek to find ways to reduce the computational cost of the algorithm.

In this chapter, our approach involves restricting attention to nominally zero-forcing beamforming directions. In that case, the structure of the integrand in (3.5b) simplifies, and this simplification facilitates a simple approximation of the integrand that enables straightforward application of residue theory to obtain an analytic expression for the integral. This approach was inspired in part by some related work in which a slightly different receiver structure was employed (Sohrabi and Davidson, 2013).

4.1 Problem Formulation in ZF Case

For the case of zero-forcing beamforming, $\mathbf{B} = \mathbf{B}_{\text{ZF}} = \hat{\mathbf{H}}^H\big(\hat{\mathbf{H}}\hat{\mathbf{H}}^H\big)^{-1}$, and hence $\bar{\mathbf{B}}_k^H\hat{\mathbf{h}}_k = \mathbf{0}$ and $\hat{\mathbf{h}}_k^H\mathbf{b}_k = 1$. These simplifications mean that we can rewrite the robust power loading problem in (2.19) as

$$\min_{\{p_k\geq 0\}} \ \mathrm{Tr}\big(\mathbf{B}_{\text{ZF}}\mathbf{P}\mathbf{B}_{\text{ZF}}^H\big) \tag{4.1a}$$

$$\text{s.t. } \Pr_{\mathbf{e}_k}\Big(\frac{|1+\mathbf{e}_k^H\mathbf{b}_k|^2 p_k}{\mathbf{e}_k^H\bar{\mathbf{B}}_k\mathbf{P}\bar{\mathbf{B}}_k^H\mathbf{e}_k+\sigma_k^2}\geq\gamma_k\Big)\geq 1-\epsilon_k, \qquad \forall k, \tag{4.1b}$$

where $\mathbf{P} = \mathrm{Diag}(p_1, p_2, ..., p_K)$, or equivalently, as

$$\min_{\{p_k\geq 0\}} \ \mathrm{Tr}\big(\mathbf{B}_{\text{ZF}}\mathbf{P}\mathbf{B}_{\text{ZF}}^H\big) \tag{4.2a}$$

$$\text{s.t. } \Pr_{\boldsymbol{\delta}_k}\Big(\boldsymbol{\delta}_k^H\mathbf{Q}_k\boldsymbol{\delta}_k + (\tfrac{p_k}{\gamma_k})2\,\mathrm{Re}(\boldsymbol{\delta}_k^H\tilde{\mathbf{r}}_k)+v_k\geq 0\Big)\geq 1-\epsilon_k, \qquad \forall k, \tag{4.2b}$$

where $\mathbf{Q}_k = \mathbf{C}_k{}^{1/2}\big(\frac{p_k}{\gamma_k}\mathbf{b}_k\mathbf{b}_k^H - \bar{\mathbf{B}}_k\mathbf{P}\bar{\mathbf{B}}_k^H\big)\mathbf{C}_k{}^{1/2}$, $\tilde{\mathbf{r}}_k = \mathbf{C}_k{}^{1/2}\mathbf{b}_k$ and $v_k = \frac{p_k}{\gamma_k} - \sigma_k^2$. Note that $\mathbf{r}_k = \frac{p_k}{\gamma_k}\tilde{\mathbf{r}}_k$; this rescaling simplifies the discussion below. The deterministic reformulation of this problem obtained by applying the results of the previous chapter is

$$\min_{\{p_k\geq 0\}} \quad \mathrm{Tr}\big(\mathbf{B}_{\text{ZF}}\mathbf{P}\mathbf{B}_{\text{ZF}}^H\big) \tag{4.3a}$$

$$\text{s.t.} \quad \frac{1}{2\pi}\int_{-\infty}^{\infty}\frac{e^{\tau_k(i\omega+\beta)}}{i\omega+\beta}\frac{e^{-c_k}}{\det(\mathbf{I}-(i\omega+\beta)\mathbf{Q}_k)}d\omega\geq 1-\epsilon_k, \qquad \forall k, \tag{4.3b}$$

where $\tau_k = -\sigma_k^2$, $c_k = \sum_{m=1}^{M}\frac{|\tilde{a}_{km}|^2(i\omega+\beta)\lambda_{mk}}{1+(i\omega+\beta)\lambda_{mk}}$ and $\mathbf{a}_k = -\mathbf{C}_k{}^{-1/2}\hat{\mathbf{h}}_k$, where if $\mathbf{Q}_k = \mathbf{V}_k\boldsymbol{\Lambda}_k\mathbf{V}_k^H$, λ_{mk} is denoting the eigenvalues of $\mathbf{Q}_k$ arranged in descending order, $\tilde{\mathbf{a}}_k = \mathbf{V}_k^H\mathbf{a}_k$ and $\tilde{a}_{km}$ is the m^{th} element of $\tilde{\mathbf{a}}_k$.

Since the ℓ^{th} term of the Taylor series expansion of e^{-c_k} has M poles of multiplicity ℓ, it is complicated to apply residue theory directly to the integral in (4.3b). However, if c_k were a constant, then the integrand would take the form of $e^{\tau_k s}G_k(s)$, where $G_k(s)$ is a rational function of $s = \beta + i\omega$. In that case, the application of residue theory is quite straightforward.

One way to approximate the probability in such a way that c_k is constant is to approximate the the linear term $2\,\mathrm{Re}(\boldsymbol{\delta}_k^H \tilde{\mathbf{r}}_k)$ by an appropriate constant value. Since $\boldsymbol{\delta}_k$ is a zero mean Gaussian random variable (RV) with identity covariance matrix, the term $2\,\mathrm{Re}(\boldsymbol{\delta}_k^H \tilde{\mathbf{r}}_k)$ is a zero mean Gaussian RV with variance $4\|\tilde{\mathbf{r}}_k\|^2$. Based on the value of $\|\tilde{\mathbf{r}}_k\|^2$, we can substitute $2\,\mathrm{Re}(\boldsymbol{\delta}_k^H \tilde{\mathbf{r}}_k)$ with a proper constant value, η_k, and then seek to solve the approximated problem.

In Section 4.5, we will discuss how to determine a reasonable value for η_k and also a possible iterative algorithm. In this section, we assume that $2\,\mathrm{Re}(\boldsymbol{\delta}_k^H \tilde{\mathbf{r}}_k)$ is replaced by a reasonable constant value, η_k, and propose the algorithm to solve the new approximated problem. With this replacement, the problem in (4.2) can be approximated by

$$\min_{\{p_k \geq 0\}} \ \mathrm{Tr}\big(\mathbf{B}_{\mathrm{ZF}}\mathbf{P}\mathbf{B}_{\mathrm{ZF}}^H\big) \tag{4.4a}$$

$$\text{s.t. } \Pr_{\boldsymbol{\delta}_k}\big(\boldsymbol{\delta}_k^H \mathbf{Q}_k \boldsymbol{\delta}_k + v_k' \geq 0\big) \geq 1 - \epsilon_k, \qquad \forall k, \tag{4.4b}$$

where $\mathbf{Q}_k = \mathbf{C}_k{}^{1/2}\big(\frac{p_k}{\gamma_k}\mathbf{b}_k\mathbf{b}_k^H - \bar{\mathbf{B}}_k\mathbf{P}\bar{\mathbf{B}}_k^H\big)\mathbf{C}_k{}^{1/2}$, $v_k' = \frac{p_k}{\gamma_k}\eta_k + v_k = \frac{p_k}{\gamma_k'} - \sigma_k^2$, and $\gamma_k' = \frac{\gamma_k}{1+\eta_k}$.

Now by taking the same steps that were taken in Chapter 3, we can convert the chance constraint in (4.4) to $\Pr(\|\boldsymbol{\delta}_k\|^2_{-\mathbf{Q}_k} \leq p_k/\gamma_k' - \sigma_k^2)$. Then, by using Lemma 1, we can convert the approximated probabilistically constrained problem to a deterministic

problem with integral constraints as, namely

$$\min_{\{p_k \geq 0\}} \quad \mathrm{Tr}\big(\mathbf{B}_{\mathrm{ZF}}\mathbf{P}\mathbf{B}_{\mathrm{ZF}}^{H}\big) \tag{4.5a}$$

$$\text{s.t.} \quad \frac{1}{2\pi}\int_{-\infty}^{\infty} \frac{e^{\tau_k(i\omega+\beta)}}{i\omega+\beta}\frac{1}{\det(\mathbf{I}-(i\omega+\beta)\mathbf{Q}_k)}d\omega \geq 1-\epsilon_k, \qquad \forall k, \tag{4.5b}$$

where $\tau_k = \upsilon'_k = \frac{p_k}{\gamma'_k} - \sigma_k^2$.

In the next section, we will show how these simplifications and approximations enable the application of residue theory to compute the integral in (4.5b) as a summation. (Residue theory was employed in a related context by Park *et al.*, 2012). This enables us to calculate the probability of success in (4.4b) in more efficient numerical way. In Section 4.3, using the results of Section 4.2, we will propose a coordinate descent algorithm which has the same structure as the algorithm of Chapter 3, but seeks to solve the approximated problem for the special case of ZF beamforming and by employing the residue representation of the integral in (4.5b), it does so with lower computational cost. Then, in Section 4.4, we subsequently apply a conservative approximation to the residue representation of the integral, and obtain a conservative power loading algorithm that has significantly lower computational cost.

4.2 Converting Integral Constraint to Summation for Approximated ZF Problem Formulation

As mentioned in previous section, we can convert the chance constraint in (4.4) to $\Pr(\|\boldsymbol{\delta}_k\|^2_{-\mathbf{Q}_k} \leq p_k/\gamma'_k - \sigma_k^2)$. By applying residue theory to the integral expression of

that chance constraint we obtain

$$\Pr\big(\|\boldsymbol{\delta}_k\|^2_{-\mathbf{Q}_k} \le p_k/\gamma'_k - \sigma_k^2\big) = \begin{cases} 1 + \sum_{\ell=1}^{r-1} f_{\ell k}(\mathbf{P}) & \text{if } p_k \ge \gamma'_k\sigma_k^2 \\ f_{rk}(\mathbf{P}) & \text{if } p_k < \gamma'_k\sigma_k^2 \end{cases} \tag{4.6}$$

where $r = \min(N_t - 1, K) + 1$,

$$f_{\ell k}(\mathbf{P}) = \begin{cases} 0 & \text{if } \lambda_{\ell k} = 0 \\ -\exp\Big(\big(\frac{1}{\gamma'_k}p_k - \sigma_k^2\big)\frac{-1}{\lambda_{\ell k}}\Big)\frac{1}{\prod_{j\neq\ell}(1-\lambda_{jk}/\lambda_{\ell k})} & \text{otherwise} \end{cases} \tag{4.7}$$

and λ_{mk} is the m^{th} largest eigenvalue of $-\mathbf{Q}_k$, the non-zero eigenvalues of which are assumed to be distinct. To prove the statement in (4.6) and (4.7), we observe that

$$\begin{aligned} &\Pr\big(\|\boldsymbol{\delta}_k\|^2_{-\mathbf{Q}_k} \le \frac{1}{\gamma'_k}p_k - \sigma_k^2\big) \\ &= \frac{1}{2\pi}\int_{-\infty}^{\infty} \frac{e^{(\frac{1}{\gamma'_k}p_k - \sigma_k^2)(i\omega+\beta)}}{i\omega+\beta}\frac{1}{\det(\mathbf{I} + (i\omega+\beta)(-\mathbf{Q}_k))}d\omega \\ &= \frac{1}{2\pi i}\int_{-i\infty+\beta}^{i\infty+\beta} \frac{e^{(\frac{1}{\gamma'_k}p_k - \sigma_k^2)s}}{s}\frac{1}{\det(\mathbf{I} + s(-\mathbf{Q}_k))}ds \\ &= \frac{1}{2\pi i}\int_{-i\infty+\beta}^{i\infty+\beta} \frac{e^{(\frac{1}{\gamma'_k}p_k - \sigma_k^2)s}}{s}\frac{1}{\prod_j(1+s\lambda_{jk})}ds. \end{aligned} \tag{4.8}$$

Note that $-\mathbf{Q}_k = {\mathbf{C}_k}^{1/2}\big(-\frac{p_k}{\gamma_k}\mathbf{b}_k\mathbf{b}_k^H + \bar{\mathbf{B}}_k\mathbf{P}\bar{\mathbf{B}}_k^H\big){\mathbf{C}_k}^{1/2}$, which is the sum of a rank $r-1 = \min(N_t-1, K)$ positive definite matrix and a rank one negative definite matrix. Given the properties of ZF beamforming, this means that $-\mathbf{Q}_k$ typically has $r-1$ positive eigenvalues and one negative eigenvalue.

In Fig. 4.1, the general shape of the location of the poles of the argument of the integral in (4.8) is illustrated. The integral in (4.8) that we are trying to evaluate is

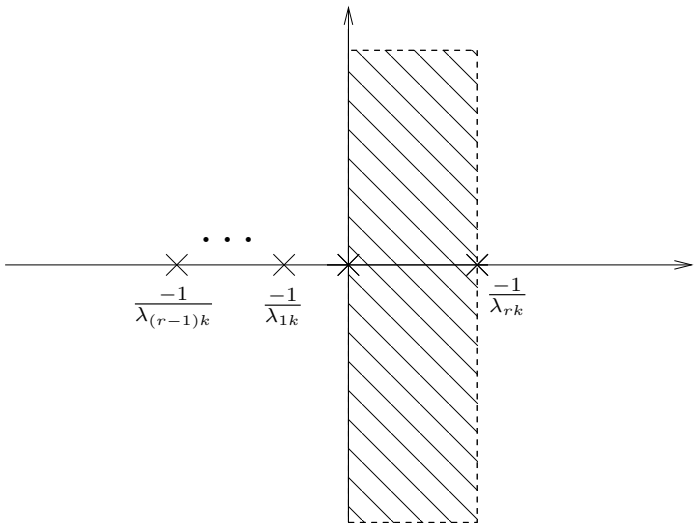

Figure 4.1: General shape of the location of the poles of the integral in (4.8).

along the vertical line with real value β. According to the Lemma 1, β can be any positive constant value that satisfies $1 + \beta\lambda_{mk} > 0$ for all m. For positive eigenvalues this constraint always holds, but for the negative eigenvalue, λ_{rk}, we must have $\beta < \frac{-1}{\lambda_{rk}}$. This condition and the fact that $\beta > 0$ require that β be chosen in the shaded region of Fig. 4.1. The next step in applying residue theory is to pick the appropriate closed contour such that the integral in (4.8) is equal to integral along that contour. For this purpose, a path should be added to complete the closed contour in such a way that the integral on the added path is zero. For finding the appropriate path to be added, the problem in divided into two cases. In the case that $p_k/\gamma'_k - \sigma_k^2 \geq 0$, the suitable contour, C_1, is depicted in Fig. 4.2, since the integrand is zero for the semicircular portion of the path. Therefore, by using the residue theory we can simplify the integral in (4.8) to

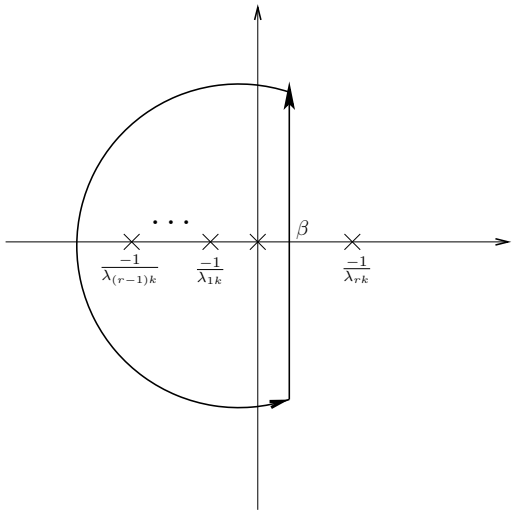

Figure 4.2: Appropriate contour for the cases that $p_k/\gamma'_k - \sigma_k^2 \geq 0$.

$$
\begin{aligned}
&\frac{1}{2\pi i}\int_{-i\infty+\beta}^{i\infty+\beta} \frac{e^{(\frac{1}{\gamma'_k}p_k-\sigma_k^2)s}}{s}\frac{1}{\prod_j(1+s\lambda_{jk})}ds \\
&= \frac{1}{2\pi i}\oint_{C_1} F(s)ds \\
&= \operatorname*{Res}_{s=0} F(s) + \sum_{\ell=1}^{r-1}\operatorname*{Res}_{s=\frac{-1}{\lambda_{\ell k}}} F(s) \\
&= 1 + \sum_{\ell=1}^{r-1}\lim_{s\to\frac{-1}{\lambda_{\ell k}}}(s+\frac{1}{\lambda_{\ell k}})\frac{e^{(\frac{1}{\gamma'_k}p_k-\sigma_k^2)s}}{s}\frac{1}{\prod_j(1+s\lambda_{jk})} \\
&= 1 + \sum_{\ell=1}^{r-1} -e^{(\frac{1}{\gamma'_k}p_k-\sigma_k^2)\frac{-1}{\lambda_{\ell k}}}\frac{1}{\prod_{j\neq\ell}(1-\frac{\lambda_{jk}}{\lambda_{\ell k}})} \\
&= 1 + \sum_{\ell=1}^{r-1} f_{\ell_k}(\mathbf{P}).
\end{aligned}
\tag{4.9}
$$

On the other hand, for the case that $p_k/\gamma'_k - \sigma_k^2 < 0$, the suitable contour, C_2, is depicted in Fig. 4.3, since the integrand is zero for semicircular portion of that path. So in this case the residue theory should be applied just one pole. Note that this time the contour is clockwise, so according to residue theory, the integral along the

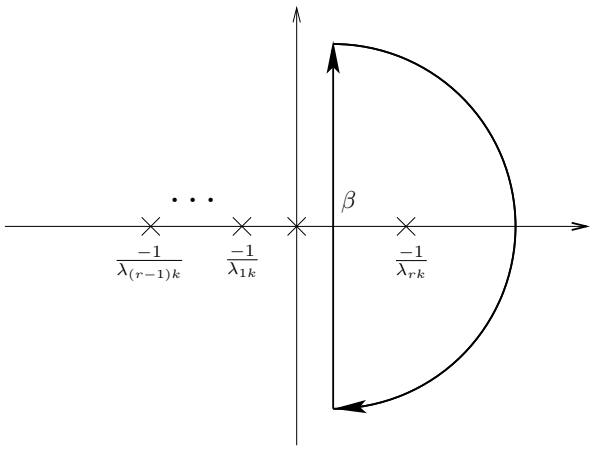

Figure 4.3: Appropriate contour for the cases that $p_k/\gamma'_k - \sigma_k^2 < 0$.

contour is equal to the negative of the residue. In this setting the integral in (4.8) can be simplified as follows

$$\begin{aligned}
&\frac{1}{2\pi i}\int_{-i\infty+\beta}^{i\infty+\beta}\frac{e^{(\frac{1}{\gamma'_k}p_k-\sigma_k^2)s}}{s}\frac{1}{\prod_j(1+s\lambda_{jk})}ds\\
&=\frac{1}{2\pi i}\oint_{C_2}F(s)ds\\
&=-\operatorname*{Res}_{\mathrm{s}=\frac{-1}{\lambda_{rk}}}F(s)\\
&=-\lim_{s\to\frac{-1}{\lambda_{rk}}}(s+\frac{1}{\lambda_{rk}})\frac{e^{(\frac{1}{\gamma'_k}p_k-\sigma_k^2)s}}{s}\frac{1}{\prod_j(1+s\lambda_{jk})}\\
&=e^{(\frac{1}{\gamma'_k}p_k-\sigma_k^2)\frac{-1}{\lambda_{rk}}}\frac{1}{\prod_{j\neq r}(1-\frac{\lambda_{jk}}{\lambda_{rk}})}\\
&=f_{rk}(\mathbf{P}).
\end{aligned}\tag{4.10}$$

Algorithm 2

Start with a feasible diagonal power allocation matrix $\mathbf{P} = \mathbf{P}^{(0)}$
for $i = 1 \rightarrow iteration_{max}$ **do**
    For all k, choose $\Delta_k^{(i)}$ such that $\Delta_k^{(i)} \leq \Delta_k^{(i-1)}$
    for $k = 1 \rightarrow K$ **do**
        Find $p_k = p_k^{(i)}$ by using bisection search such that:
        $\{p_k^{(i)} \in (0, p_k^{(i-1)}] \mid 1 - \epsilon_k \leq \Pr\big(\delta_k^H \mathbf{Q}_k \boldsymbol{\delta}_k + v_k' \geq 0\big) \leq 1 - \epsilon_k + \Delta_k^{(i)}\}$
    end for
    if $\forall k;\ 1 - \epsilon_k \leq \Pr\big(\delta_k^H \mathbf{Q}_k \boldsymbol{\delta}_k + v_k' \geq 0\big) \leq 1 - \epsilon_k + \Delta_k^{\min}$ **then**
        STOP
    end if
end for

4.3 Coordinate Descent Algorithm for ZF

A straight forward approach to exploiting the analysis in this chapter in the downlink design problem is simply to replace integral calculation in the previous chapter by the approximated residue calculation obtained in previous section. The algorithm is very similar to the algorithm in previous chapter, and is simply stated in Algorithm 2. The only difference with the general case is that the probability of success is evaluated by (4.6), and using this expression requires fewer operations than evaluating the integral in (4.5b). In Section 4.5, we will describe how to choose η_k in a sensible way such that solving the approximated problem by this algorithm is equivalent to solving the original problem with high probability.

4.4 New Algorithm for Power Allocation Update Based on Essence of Probability of Success

In this section, we use the probability of success formula in (4.6) to develop a different approach to finding good power allocations for the problem in (4.4). Unlike our previous algorithms, which start from a feasible point and then seek to reduce each power in turn in such a way that power allocation remains feasible, this method starts from a power allocation that is not necessarily feasible. Using the iterative algorithm described in this section, the power allocation is iteratively updated in such a way that it often converges to a good solution.

To begin the development of the algorithm, we observe that in the residue expression of the integral in (4.6), $f_{\ell_k}(\mathbf{P})$, is a function of p_k, through the eigenvalues of $-\mathbf{Q}_k$, and this relationship is hard to express analytically. This complicates the development of a cyclic coordinate update algorithm. To address that difficulty, at the k^{th} step of the i^{th} cycle we will construct an approximation of $\mathbf{Q}_k^{(i)}$ as $\hat{\mathbf{Q}}_k^{(i)} = {\mathbf{C}_k}^{1/2}\big(\frac{p_k^{(i-1)}}{\gamma_k}\mathbf{b}_k\mathbf{b}_k^H - \bar{\mathbf{B}}_k\mathbf{P}_k^{(i-1)}\bar{\mathbf{B}}_k^H\big){\mathbf{C}_k}^{1/2}$. There are two variations on how to construct $\mathbf{P}_k^{(i-1)}$. We can construct $\mathbf{P}_k^{(i-1)}$ based on the power allocations in previous cycle for all users; i.e., $\mathbf{P}_k^{(i-1)} = \mathbf{P}^{(i-1)} = \text{Diag}(p_1^{(i-1)}, p_2^{(i-1)}, \ldots, p_K^{(i-1)})$. The alternative way is to use the updated powers of the current cycle for prior users and previous cycle power allocations for the rest; i.e., $\mathbf{P}_k^{(i-1)} = \text{Diag}(p_1^{(i)}, \ldots, p_{k-1}^{(i)}, p_k^{(i-1)}, p_{k+1}^{(i-1)}, \ldots, p_K^{(i-1)})$. Although the second choice may result in less cycles, our numerical results suggest that constructing $\hat{\mathbf{Q}}_k^{(i)}$ based on the first choice of $\mathbf{P}_k^{(i-1)}$ leads to a faster algorithm since the $\hat{\mathbf{Q}}_k^{(i)}$ and its eigenvalues are evaluated only once in each cycle.

According to the strategy in the previous chapter, we are looking for a power

allocation near the boundary of feasible set. At the k^{th} step of the i^{th} cycle, the design problem becomes $\min_{p_k^{(i)} \geq 0} p_k^{(i)}$ subject to

$$\begin{cases} 1 + \sum_{\ell=1}^{r-1} \hat{f}_{\ell k}(p_k^{(i)}) \geq 1 - \epsilon_k & \text{if } p_k^{(i)} \geq \gamma_k' \sigma_k^2 \\ \hat{f}_{rk}(p_k^{(i)}) \geq 1 - \epsilon_k & \text{if } p_k^{(i)} < \gamma_k' \sigma_k^2 \end{cases}, \tag{4.11}$$

where

$$\hat{f}_{lk}(p_k^{(i)}) = \begin{cases} 0 & \text{if } \hat{\lambda}_{\ell k}^{(i)} = 0 \\ -\exp\Big((\frac{1}{\gamma_k'} p_k^{(i)} - \sigma_k^2) \frac{-1}{\hat{\lambda}_{\ell k}^{(i)}} \Big) \frac{1}{\prod_{j \neq \ell} (1 - \hat{\lambda}_{jk}^{(i)} / \hat{\lambda}_{\ell k}^{(i)})} & \text{otherwise} \end{cases}, \tag{4.12}$$

and $\hat{\lambda}_{mk}^{(i)}$ is the m^{th} largest eigenvalue of $-\hat{\mathbf{Q}}_k^{(i)}$. Here we have assumed that the non-zero eigenvalues are distinct.

Since we are looking for the smallest $p_k^{(i)}$, we first consider the second case in (4.11) where $p_k^{(i)} < \gamma_k' \sigma_k^2$. In this case we look for the smallest $p_k^{(i)}$ that satisfies $\hat{f}_{rk}(p_k^{(i)}) \geq 1 - \epsilon_k$, which is equivalent to

$$p_k^{(i)} \geq \gamma_k' \sigma_k^2 - \gamma_k' \hat{\lambda}_{rk}^{(i)} \ln\Big((1 - \epsilon_k) \prod_{j \neq r} (1 - \hat{\lambda}_{jk}^{(i)} / \hat{\lambda}_{rk}^{(i)}) \Big). \tag{4.13}$$

Since we seek small powers, $p_k^{(i)}$ is chosen such that equality holds in (4.13). This $p_k^{(i)}$ is acceptable when it lies in the interval of $(0, \gamma_k' \sigma_k^2)$, which is the assumption that underlies the derivation of (4.13). Our numerical experiments show that this condition is not satisfied very often. Therefore, most of the time the other case should be considered.

For the other case in (4.11), the desired solution is simply the smallest non-negative root of $\sum_{\ell=1}^{r-1} \hat{f}_{\ell k}(p_k^{(i)}) + \epsilon_k = 0$. Since $\hat{f}_{\ell k}(p_k^{(i)})$ is smooth, a number of root finding algorithms could be considered. Instead of doing that, we will employ a conservative approximation of the constraint $1 + \sum_{\ell=1}^{r-1} \hat{f}_{\ell k}(p_k^{(i)}) \geq 1 - \epsilon_k$ and show that the resulting problem has a closed-form solution. As ℓ increases, the argument of the exponential in (4.6) becomes more negative, and hence the magnitude of $\hat{f}_{\ell k}(p_k^{(i)})$ decreases. Furthermore, for odd ℓ, $\hat{f}_{\ell k}(p_k^{(i)}) < 0$, whereas for even ℓ, $\hat{f}_{\ell k}(p_k^{(i)}) > 0$. As a result we have that $\sum_{\ell=2}^{r-1} \hat{f}_{\ell k}(p_k^{(i)}) \geq 0$ and that this term will typically be small in comparison to $|\hat{f}_{1k}(p_k^{(i)})|$. Therefore, if $p_k^{(i)}$ is chosen such that $1 + \hat{f}_{1k}(p_k^{(i)}) \geq 1 - \epsilon_k$, then the outage constraint is guaranteed to hold. More explicitly, $p_k^{(i)}$ is chosen such that

$$p_k^{(i)} \geq \gamma_k \sigma_k^2 - \gamma_k \hat{\lambda}_{1k}^{(i)} \ln\Big(\epsilon_k \prod_{j \neq 1} (1 - \hat{\lambda}_{jk}^{(i)} / \hat{\lambda}_{1k}^{(i)})\Big). \tag{4.14}$$

Since we seek small powers, $p_k^{(i)}$ is chosen such that equality holds in (4.14).

To initialize the algorithm, we chose $p_k^{(0)}$ as if we have equal power allocation with the k^{th} user's parameters. This assumption is based on the insight of Sohrabi and Davidson (2013) for a slightly different system. For the system considered by Sohrabi and Davidson (2013), equal power allocation is optimal in the scenario in which all users have the same σ, γ, $\mathbf{C}$ and ϵ. However, for the SINR definition which is used in this thesis, that is not the case. Despite that, we still use the same method for selecting $p_k^{(0)}$. That is, we choose

$$p_k^{(0)} = \frac{\sigma_k^2}{1/\gamma_k' + \tilde{\lambda}_{1k} \ln\big(\epsilon_k \prod_{j \neq 1} (1 - \tilde{\lambda}_{jk} / \tilde{\lambda}_{1k})\big)} \quad \forall k, \tag{4.15}$$

where $\tilde{\lambda}_{mk}$ is the m^{th} largest eigenvalue of the corresponding $-\tilde{\mathbf{Q}}_k = -{\mathbf{C}_k}^{1/2}\big(\frac{1}{\gamma_k}\mathbf{b}_k\mathbf{b}_k^H -$

$\bar{\mathbf{B}}_k\bar{\mathbf{B}}_k^H\big)\mathbf{C}_k{}^{1/2}$. Unlike the coordinate descent algorithm in previous chapter and that in Section 4.3, this initial power allocation is not necessarily feasible, but as the coordinates are updated, the power allocation tends to move toward the feasible set. The cyclic updates are terminated once a feasible point is found or if no feasible point is found in a reasonable time. (Feasibility is evaluated using the expression in (4.6) and comparing with $1-\epsilon_k$.) Our numerical experience suggests that the starting point in (4.15) is particularly effective in that the level of conservatism in the first feasible point tends to be low. In structures where that is not the case, one can use this feasible point to initialize the algorithm in Section 4.3.

4.5 Discussion on How to Choose η_k

In the ZF beamforming case, $\Pr\big(\mathsf{SINR_k} \geq \gamma_k\big) \geq 1-\epsilon_k$, can be written as

$$\Pr\Big(\boldsymbol{\delta}_k^H\mathbf{Q}_k\boldsymbol{\delta}_k + (\tfrac{p_k}{\gamma_k})2\,\mathrm{Re}(\boldsymbol{\delta}_k^H\tilde{\mathbf{r}}_k) + v_k \geq 0\Big) \geq 1-\epsilon_k. \tag{4.16}$$

In this chapter, we have approximated this constraint by replacing the term $2\,\mathrm{Re}(\boldsymbol{\delta}_k^H\tilde{\mathbf{r}}_k)$ by a constant η_k. That is, we have employed the constraint

$$\Pr\Big(\boldsymbol{\delta}_k^H\mathbf{Q}_k\boldsymbol{\delta}_k + (\tfrac{p_k}{\gamma_k})\eta_k + v_k \geq 0\Big) \geq 1-\epsilon_k. \tag{4.17}$$

In this section, we seek guidelines for the choice of η_k.

To begin, we observe that the probability on the left hand side of (4.17) is a increasing function of η_k. However, the probability that $2\,\mathrm{Re}(\boldsymbol{\delta}_k^H\tilde{\mathbf{r}}_k) \geq \eta_k$ is a decreasing function of η_k. To analyze this in more detail, in Appendix B we show that if we are

able to design power allocation such that $\Pr\Big(\boldsymbol{\delta}_k^H \mathbf{Q}_k \boldsymbol{\delta}_k + (\frac{p_k}{\gamma_k})\eta_k + v_k \geq 0\Big) \geq 1 - \epsilon_k$, then the probability that the SINR meets the specified target, $\Pr\big(\mathsf{SINR_k} \geq \gamma_k\big)$, can be lower bounded as

$$\Pr\big(\mathsf{SINR_k} \geq \gamma_k\big) = \Pr\Big(\boldsymbol{\delta}_k^H \mathbf{Q}_k \boldsymbol{\delta}_k + (\tfrac{p_k}{\gamma_k}) 2\,\mathrm{Re}(\boldsymbol{\delta}_k^H \tilde{\mathbf{r}}_k) + v_k \geq 0\Big) \geq \rho_k(\eta_k) - \epsilon_k + I'(\eta_k), \tag{4.18}$$

where $\rho_k(\eta_k) = \Pr\big(2\,\mathrm{Re}(\boldsymbol{\delta}_k^H \tilde{\mathbf{r}}_k) \geq \eta_k\big)$ and hence is a decreasing function of η_k and $I'(\eta_k)$ is positive increasing function of η_k. The lower bound in (4.18) illustrates one aspect of the trade off in selecting η_k. It is tempting to consider choosing η_k so that $\rho_k(\eta_k)$ is large, as this increases the probability that designing a power loading that satisfies the approximated QoS constraint in (4.17) produces a power loading that satisfies the original QoS constraint in (4.16). Indeed, since $2\,\mathrm{Re}(\boldsymbol{\delta}_k^H \tilde{\mathbf{r}}_k)$ is a zero mean Gaussian random variable of variance $4\|\tilde{\mathbf{r}}_k\|^2$, it is tempting to choose $\eta_k = -3 \times 2\|\tilde{\mathbf{r}}_k\|$. However, doing so is inherently conservative. In particular, the approximated problem maybe infeasible when the original problem is, in fact, feasible.

To make progress on the choice of η_k, we have examined η_k in the form

$$\eta_k = -\eta'_k \times 2\|\tilde{\mathbf{r}}_k\|. \tag{4.19}$$

In Fig. 4.4 we have provided a typical plot from those experiments. The actual feasibility rate in the figure is the percentage of problem instances for which the approximated problem generates a solution that is feasible for the original problem. This was generated for the environment described in Appendix C. That figure shows the benefits of increasing η'_k so that it is more likely that $2\,\mathrm{Re}(\boldsymbol{\delta}_k^H \tilde{\mathbf{r}}_k) \geq \eta_k$ increase rapidly for small η'_k, but then begin to degrade once η_k reaches a threshold because the

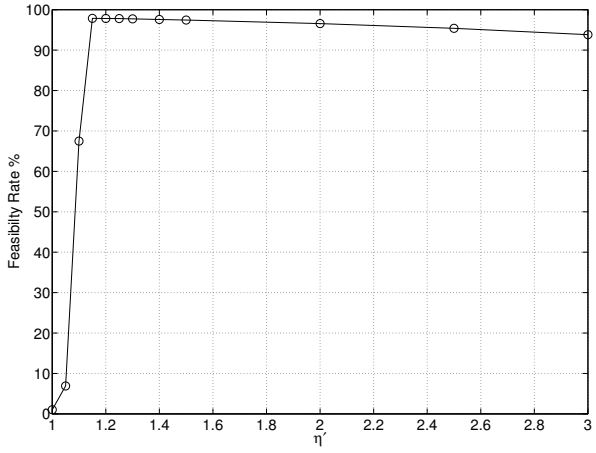

Figure 4.4: Actual feasibility rate against η' in the environment where $N_t = K = 3$, $\mathbf{C} = 0.002\mathbf{I}$, $\sigma^2 = 0.01$, $\epsilon = 0.05$, $\gamma = 3$ dB.

constraint in (4.17) becomes overly conservative. This is consistent with our earlier observations.

Rather than fixing η_k to a particular value, an alternative approach is to change it iteratively based on an evaluation of whether or not the current power loading satisfies the original QoS constraint. (This can be tested using the integral expression in (4.3b), which is the specialization of the expression in (3.5b) to the ZF case.) If the current power loading does not satisfy the original QoS constraints, η_k should be decreased (or η'_k in (4.19) increased), whereas if the current power loading over-satisfies the original QoS constraint η_k can be increased (or η'_k in (4.19) decreased). As will be seen in the experiments in Chapter 5, this enables us to achieve power loadings that are close to the boundary of the feasible set and hence result in low transmission power.

Chapter 5

Performance Evaluation

In this chapter, we demonstrate the performance of the proposed algorithms.

In the study of our general algorithm in Chapter 3, we use regularized channel inversion (RCI) beamforming; i.e., $\mathbf{B}_{\mathrm{RCI}} = \hat{\mathbf{H}}^H\big(\hat{\mathbf{H}}\hat{\mathbf{H}}^H + \alpha\mathbf{I}_K\big)^{-1}$ and zero-forcing beamforming; i.e., $\mathbf{B}_{\mathrm{ZF}} = \hat{\mathbf{H}}^H\big(\hat{\mathbf{H}}\hat{\mathbf{H}}^H\big)^{-1}$ as the examples of fixed-direction beamformers. For the RCI case, we specify the regularization parameter, α, according to the results of Peel *et al.* (2005) for the full CSI case. The value of α is given in Table 5.1.

To study the algorithms proposed in Chapter 4, which seek to solve the approximated problem in (4.4) for the zero-forcing case, we provide four different approaches. Two of them implement the coordinate descent algorithm proposed in Section 4.3, one having a pre-specified value of η_k while the other iteratively changes the value of η_k as described in Section 4.5. The other two demonstrate the algorithm for power allocation based on the essence of the probability of success described in Section 4.4. Again, one has a specific value for η_k while the other iteratively changes that value. In the schemes in which η_k should be pre-specified, we choose a reasonable value according to the analysis in Appendix C. The values are given in Table 5.1.

In order to compare our algorithms to the existing methods, we consider the chance-constrained robust precoding method based on the rank-one relaxation (RAR) method of Wang *et al.* (2011), which was formulated in (2.18). We also compare against the robust power loading adaptation of the approach of Wang *et al.* (2011) that was formulated in (2.23). For solving these two convex problems, we use the conic optimization solver SeDuMi, implemented through the now popularized and convenient parser software CVX (Grant and Boyd, 2012).

A summary of methods that will be considered is provided in Table 5.1.

In the following simulations, we consider an environment with $N_t = 3$ transmit antennas, $K = 3$ users, i.i.d. Rayleigh fading channels, and the receivers' noise sources are modeled as zero-mean, additive, white, and Gaussian with variance $\sigma_k^2 = \sigma^2 = 0.01$. According to the results of Section 2.1 for TDD systems in the case of i.i.d. Rayleigh fading channels, the uncertainty in the channel estimation can be modeled by a Gaussian random vectors with zero mean and covariance $\mathbf{C}_k = \mathbf{C} = \sigma_e^2\mathbf{I}$. In addition, the probability of outage is set to be $\epsilon_k = \epsilon = 0.05$ for all users and a universal SINR target is defined; i.e., $\gamma_k = \gamma$.

5.1 Actual SINR Satisfaction for Randomly Generated Gaussian Error

In this section, we examine the actual probability with which the SINR target is satisfied, i.e., $\text{Prob}\big(\mathsf{SINR}_k \geq \gamma_k\big)$, for the various methods. We fixed the QoS requirement for all users to be 3 dB; i.e., $\gamma_k = \gamma = 3$ dB and set $\sigma_e^2 = 0.002$. The histograms of the actual SINR satisfaction probabilities over different channel realizations are

Table 5.1: Description of methods.

Method	Description
RCI-General-Method ($\alpha = 0.03$)	Robust power loading (RPL) algorithm in the RCI direction with RCI parameter, $\alpha = 0.03$ that seeks to solve the problem in (3.5) according to Algorithm 1 in Chapter 3.
ZF-General-Method	RPL algorithm in the ZF direction that seeks to solve the problem in (3.5) according to Algorithm 1 in Chapter 3.
ZF-App-CordDescent-Fixed($\eta' = 1.3$)	RPL algorithm in the ZF direction that seeks to solve the approximated problem in (4.4) according to Algorithm 2 in Section 4.3, where $\eta_k = -\eta' \times 2\|\tilde{\mathbf{r}}_k\|$ and $\eta' = 1.3$.
ZF-App-CordDescent-Iterative(η_k)	RPL algorithm in the ZF direction that seeks to solve the approximated problem in (4.4) according to Algorithm 2 in Section 4.3, where η_k iteratively changes as described in Appendix D.
ZF-App-CordUpdate-Fixed($\eta' = 1.3$)	RPL algorithm in the ZF direction that seeks to solve the approximated problem in (4.4) according to the method proposed in Section 4.4, where $\eta_k = -\eta' \times 2\|\tilde{\mathbf{r}}_k\|$ and $\eta' = 1.3$.
ZF-App-CordUpdate-Iterative(η_k)	RPL algorithm in the ZF direction that seeks to solve the approximated problem in (4.4) according to the method proposed in Section 4.4, where η_k iteratively changes as described in Appendix D.
RAR	Robust precoding based on the rank-one relaxation/convex restriction method of Wang *et al.* (2011). The resulting SDP was formulated in (2.18).
ZF SDP	RPL algorithm in the ZF direction using the adaptation of the RAR method of Wang *et al.* (2011) to the case of power loading that was formulated in (2.23).

shown in Fig. 5.1. In order to obtain those histograms, we generated 500 realizations of the set of channel estimates $\{\hat{\mathbf{h}}_k^H\}_{k=1}^K$ such that for each set all methods claim that the problem is solved. Then, for each set of channel estimates realization, the actual SINR satisfaction probabilities of all methods were numerically evaluated using 100,000 randomly generated realizations of the CSI errors $\{\mathbf{e}_k\}_{k=1}^K$.

The histogram shows some of the inherent properties of the proposed algorithms. For the case of the general algorithm of Chapter 3, and also the algorithms of Chapter 4 that adapt the value of η_k, the actual SINR satisfaction probabilities are clustered close to $1-\epsilon_k$. Note that for these algorithms, the algorithm parameter was set to be $\Delta_k^{\min} = \Delta_k^{(i)} = \Delta = 0.005$, which means the algorithms are stopped when all probabilities of success lie in $[0.95, 0.955]$ or the number of iterations exceed the maximum allowed iteration. The maximum number of iterations was set to be 50 in the simulations. As such, the proposed methods are not very conservative.

In contrast, the two methods that employ convex restrictions of the original problem are quite conservative; the probability of satisfying the constraint is close to 1. (Recall that in addition to that restriction, the RAR method involves a rank-one relaxation which is almost always tight.)

For the other two methods proposed in Chapter 4, which solve the approximated problem in zero-forcing case for pre-specified $\eta' = 1.3$ where $\eta_k = -\eta' \times 2\|\tilde{\mathbf{r}}_k\|$, the actual SINR satisfaction probabilities cannot be controlled to be as close as we want to $1-\epsilon_k$, but the histograms show that those methods are not as conservative as convex restriction methods.

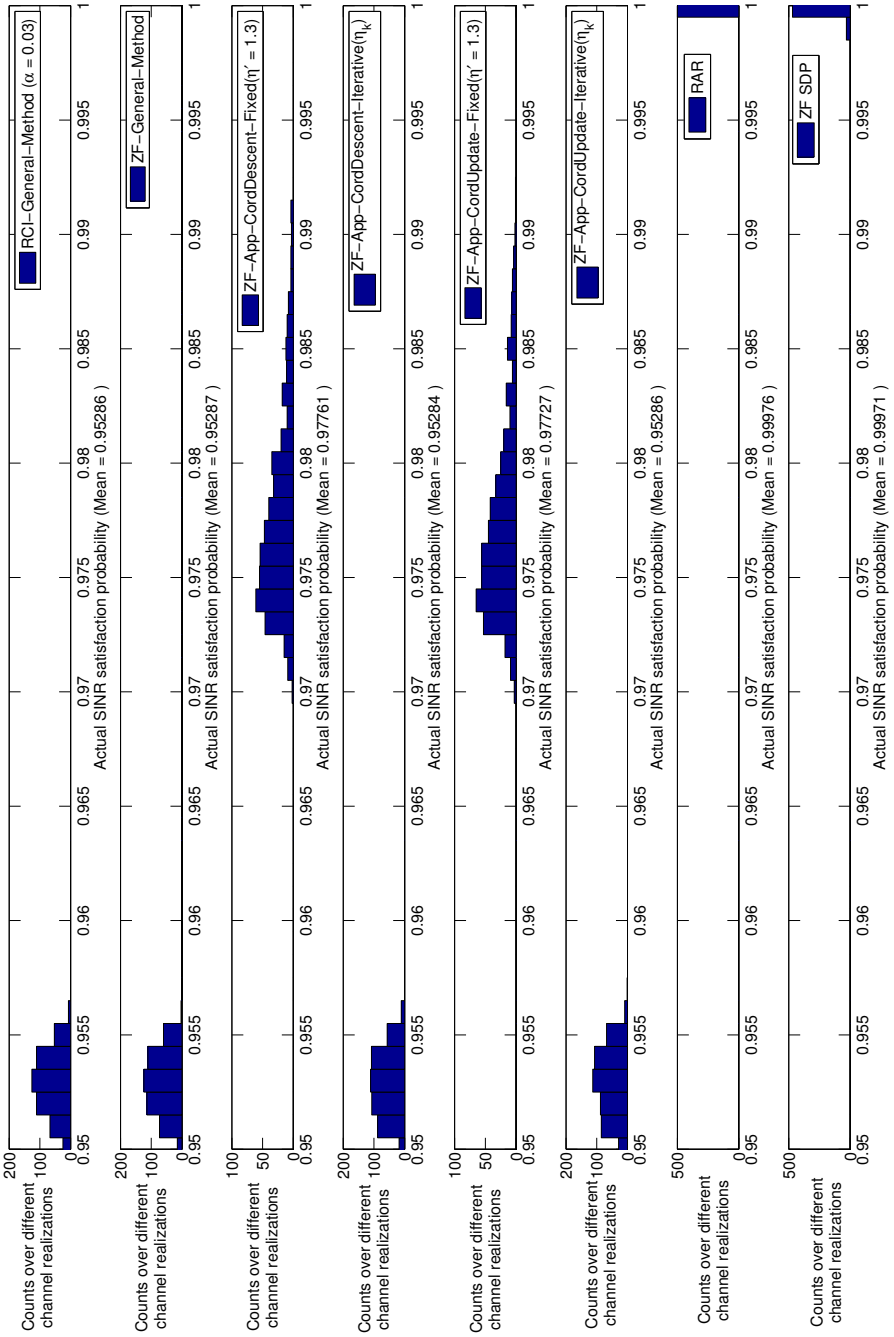

Figure 5.1: Histograms of the actual SINR satisfaction for different methods in a scenario in which $N_t = K = 3$, $\mathbf{C} = 0.002\mathbf{I}$, $\gamma = 3$ dB, $\epsilon = 0.05$, $\sigma^2 = 0.01$.

5.2 Performance Comparisons Against SINR Requirements

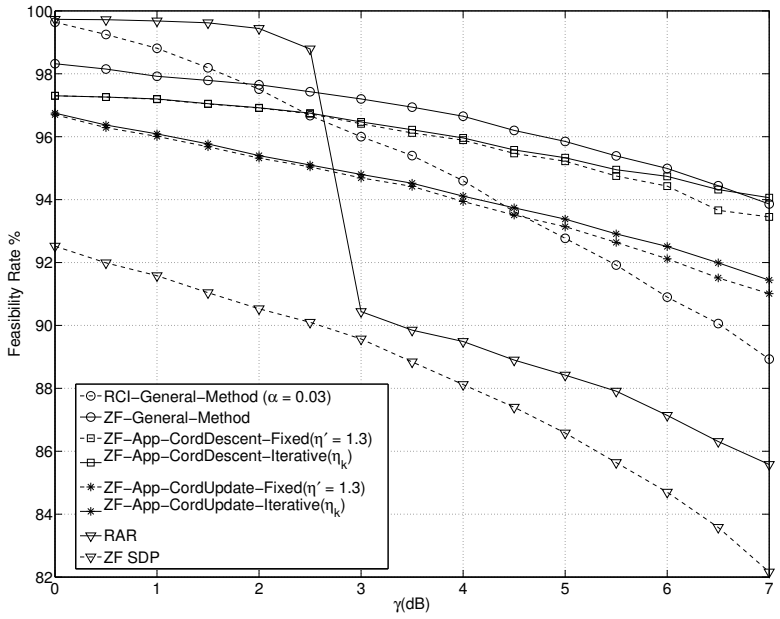

Figure 5.2: Feasibility performance for different methods in the environment where $N_t = K = 3$, $\mathbf{C} = 0.002\mathbf{I}$, $\epsilon = 0.05$, $\sigma^2 = 0.01$.

In this section, we randomly generated 10,000 realizations of the set of i.i.d. Rayleigh fading channels $\{\mathbf{h}_k^H\}_{k=1}^K$. In the uplink training phase, we assumed that there were no peak power constraints on the uplink and we set $L_1 = 1$ and $P^{\mathrm{UT}} = 4.99$ so that with the noise variance at the base station being $\sigma_{\mathrm{BS}}^2 = 0.01$, the variance of the channel estimate is $\sigma_e^2 = 0.002$. (The choice of $L_1 = 1$ is consistent with the results of Hassibi and Hochwald (2003).) We examined the performance of each method as the SINR requirement of the users, γ, increases from 0 dB to 7 dB. For each set of channel estimates and for each value of γ, we determine whether each design

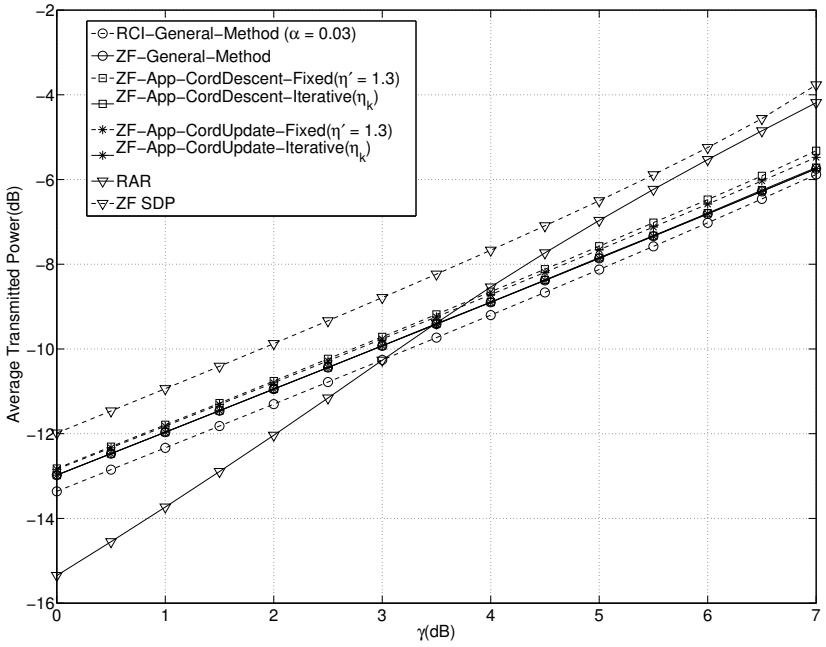

Figure 5.3: Power transmission performance for different methods in the environment where $N_t = K = 3$, $\mathbf{C} = 0.002\mathbf{I}$, $\epsilon = 0.05$, $\sigma^2 = 0.01$.

formulation generates a power loading that guarantees that the probabilistic SINR constraints are satisfied. In Fig. 5.2, we plot the percentage of channel realizations for which each design generated a feasible solution. Then, we subsequently selected all the realizations from the set of 10,000 for which all methods provide a feasible solution for all simulated SINR targets. In Fig. 5.3, we plot the average transmission power over the 8,216 such channels against γ.

From Fig. 5.2, it can be seen that by tackling the power loading problem directly (or closely), even with suboptimal algorithms, the proposed power loading methods are able to satisfy the QoS constraints more often than the existing power loading method which is based on optimal solutions to tractable conservative approximations

of the problem. This is because the approximations made in that method are quite conservative. What is perhaps more interesting is that for higher SINR targets, the proposed power loading methods provide better performance than the robust precoding method of Wang *et al.* (2011), which is formulated in (2.18), despite the fact that that method has many more degrees of design freedom. (It designs the beamformers and power allocation jointly, in contrast to the proposed methods in which the beamformers are fixed.) Once again, this is due to the fact that the techniques used in the proposed method for zero-forcing directions to convert the chance constraints to deterministic constraints are much less conservative.

5.3 Performance Comparisons Against Uncertainty Size

In the experiments in this section, we randomly generated 1,000 realizations of the set of i.i.d. Rayleigh fading channels $\{\mathbf{h}_k^H\}_{k=1}^K$, and similar to the privious simulation, we obtained the CSI at the BS through uplink training. Analogous to the experiment in Section 5.2, we chose $L_1 = 1$ and chose P^{UT} such that required channel uncertainty size, σ_e^2, is produced according to (2.10). In this experiment we set the SINR target of the users to 3 dB. Then, we seek to plot feasibility rate and average transmission power as described in previous section; see Fig. 5.4 and Fig. 5.5, respectively. Note that we plot the average transmitted power for 400 sets of channels for which all methods provide feasible solution.

It can be seen from Fig. 5.4 and Fig. 5.5, the two methods based on conservative convex restriction (RAR and ZF SDP) have poor performance as the size of the

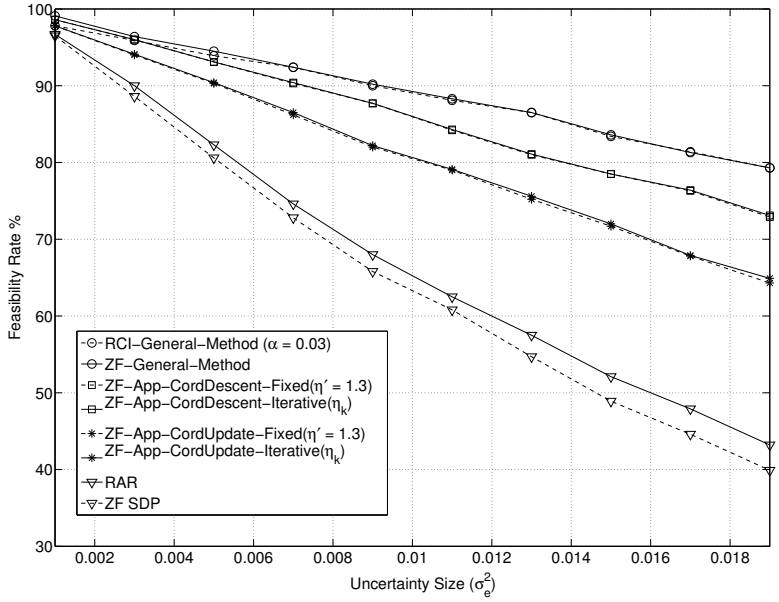

Figure 5.4: Feasibility performance for different methods in the environment where $N_t = K = 3$, $\gamma = 3$ dB, $\epsilon = 0.05$, $\sigma^2 = 0.01$.

uncertainty, σ_e^2, increases. This is caused by the fact that in the large uncertainity scenarios, the original problem is hard to solve; i.e., the feasible set in that case is small. Therefore, taking a conservative restriction step can cause the feasible set of the approximated problem to vanish. Hence, the feasibility rate is degraded, as illustrated in Fig. 5.4. Even when the feasible set does not vanish, it is sometimes made quite small. This results in large transmission power being required, as illustrated in Fig. 5.5. On the other hand, the proposed algorithms try to tackle the original problem directly (or closely), and these figures demonstrate that the resulting techniques have better performance.

Among of our proposed algorithms, the algorithms of Chapter 3 have the best performance. That is expected, because they seek to tackle original problem without any approximation. The difficulty with these methods is the computational cost of

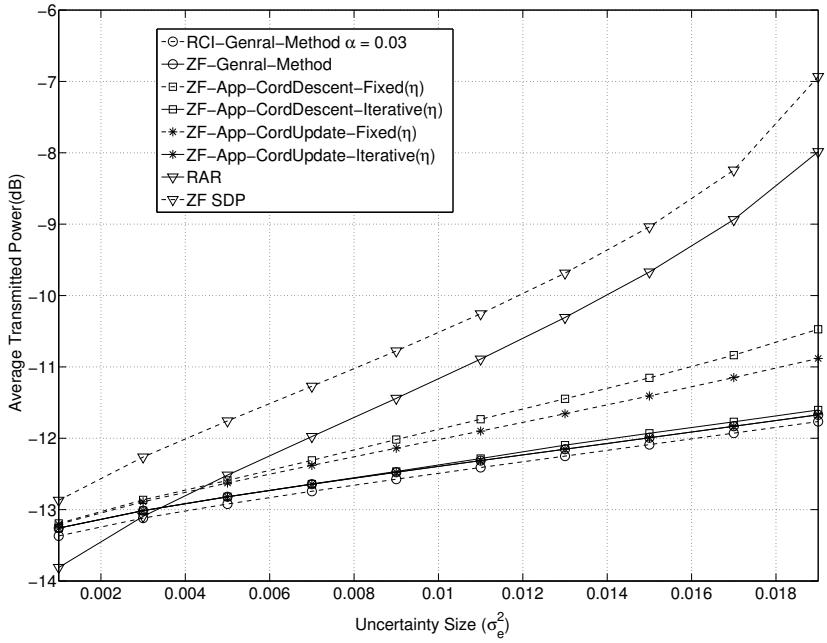

Figure 5.5: Power transmission performance for different methods in the environment where $N_t = K = 3$, $\gamma = 3$ dB, $\epsilon = 0.05$, $\sigma^2 = 0.01$.

calculating several integrals.

The two methods that seek to solve the approximated problem in Section 4.3 have the next best performance. In these methods, for each value of η' the approximated problem is guaranteed to be solved if we find the initial feasible point. This enhances the feasibility rate performance of these methods compare to the other category which are proposed in Section 4.4. The other interesting fact about all of those algorithms that seek to solve approximated problem is that by choosing a good value for η' based on Appendix C, the feasibility rate is very close to the case that the algorithms are able to change η' as illustrated in Fig. 5.4. However, the ability to change η' enhances the performance of the algorithms in the sense of transmission power, as shown in Fig. 5.5.

5.4 User Selection

In the previous simulations, the algorithms are forced to design the precoder such that the requested QoS of all three users in the network is satisfied. However, in practical systems the design of the precoder may be facilitated by user selection module to enhance the performance of the network. In other words, utilization of user selection can improve the feasibility rate and decrease the required power consumption.

In this section, we seek to implement a very simple algorithm for user selection to illustrate the improvement in the performance of the system that user selection can provide. We simulate exactly the same scenarios as in Sections 5.2 and 5.3, but instead of having three users in the network we have four users and the BS decides to communicate to three of them. The problem of which users to communicate to is an inherently combinational one, and hence would require the previous problems to be solved four times if we were to solve the problem precisely. Instead, we will use a simple heuristic to determine the user to which the base station will not transmit. The heuristic is to avoid the maximum inner product between the channel estimates of the different users, as it is difficult to communicate simultaneously to users whose channels have similar directions. Among the two users whose channel estimate inner product is the largest, we eliminate the user with the channel estimate that has smaller norm.

For analyzing performance against SINR requirement, we consider an environment where $N_t = 3$, $\sigma_e^2 = 0.002$, $\sigma^2 = 0.01$, $\epsilon = 0.05$ and the BS should communicate to $K = 3$ users out of four available users in the network, which is basically the same environment as in Section 5.2 except that the BS is provided with user selection module. The experiment is performed over 10,000 sets of channels realization. In

Figs. 5.6 and 5.7, the feasibility rate and average transmitted power are illustrated. Note that the average transmission power is depicted for the $9,182$ sets of channels for which all methods provide a feasible solution.

For analyzing performance against channel uncertainty size, we consider an environment where $N_t = 3$, $\gamma = 3$ dB, $\sigma^2 = 0.01$, $\epsilon = 0.05$ and the BS should communicate to $K = 3$ users out of four available users in the network, which is basically the same environment as in Section 5.3 except for the presence of the user selection module. The experiment is done over 1,000 sets of channels realizations. The feasibility rate and average transmitted power are illustrated in Figs. 5.8 and 5.9, respectively. (The average transmission power is depicted for the 582 sets of channels for which all methods provide a feasible solution.)

By comparing these results with previous sections, we can see the effect of user selection — it enables the QoS requirements to be achieved in more of the difficult scenarios, i.e., scenarios with high SINR targets or large CSI uncertainty. In Appendix E, we compare our heuristic user selection approach with exhaustive search among all possible sets of three users, which has the best performance among the user selection approaches. Although that comparison shows that there is a gap between the performance of our user selection heuristic and exhaustive search, the experiments in this section show that even our simple heuristic leads to significant gains over systems that they do not perform user selection.

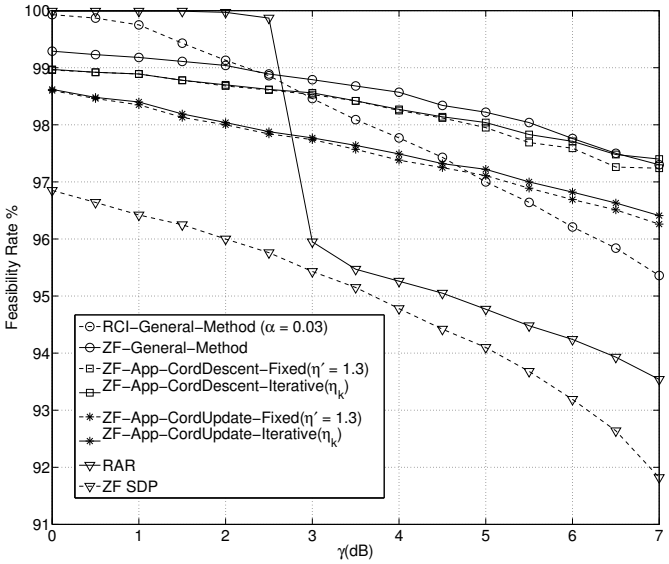

Figure 5.6: Feasibility performance for different methods in the environment where $N_t = 3$, $\mathbf{C} = 0.002\mathbf{I}$, $\sigma^2 = 0.01$, $\epsilon = 0.05$ and the BS employs a simple user selection algorithm to pick $K = 3$ users of four available users in the network.

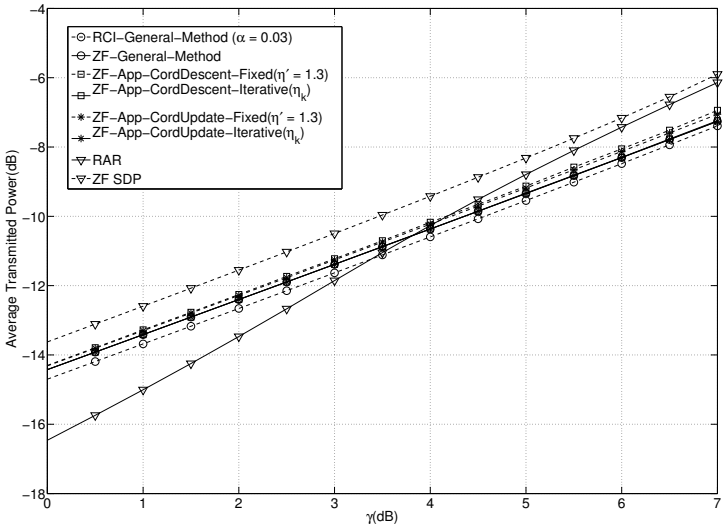

Figure 5.7: Power transmission performance for different methods in the environment where $N_t = 3$, $\mathbf{C} = 0.002\mathbf{I}$, $\sigma^2 = 0.01$, $\epsilon = 0.05$ and the BS employs a simple user selection algorithm to pick $K = 3$ users of four available users in the network.

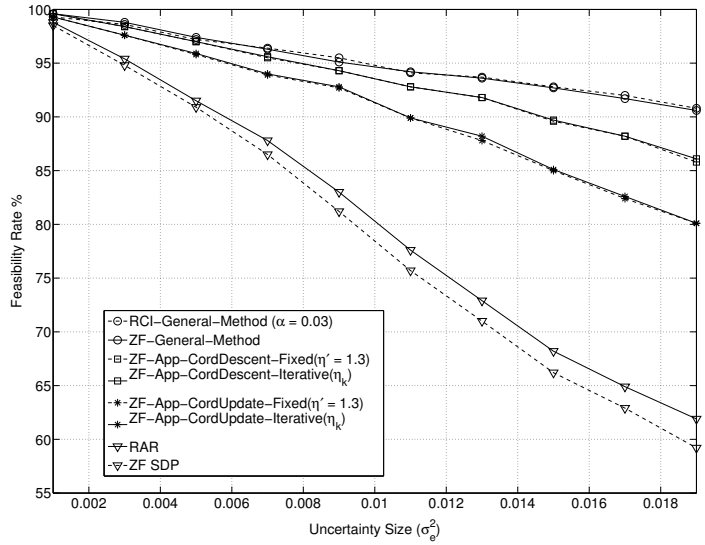

Figure 5.8: Feasibility performance for different methods in the environment where $N_t = 3$, $\gamma = 3$ dB, $\sigma^2 = 0.01$, $\epsilon = 0.05$ and the BS employs a simple user selection algorithm to pick $K = 3$ users of four available users in the network.

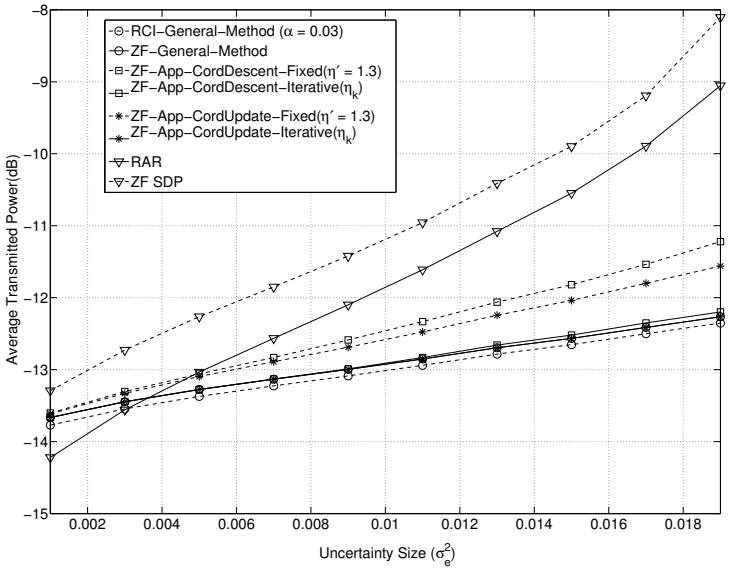

Figure 5.9: Power transmission performance for different methods in the environment where $N_t = 3$, $\gamma = 3$ dB, $\sigma^2 = 0.01$, $\epsilon = 0.05$ and the BS employs a simple user selection algorithm to pick $K = 3$ users of four available users in the network.

Chapter 6

Conclusions and Future Work

6.1 Conclusions

This thesis considered the problem of robust power loading for the MISO downlink beamforming scenario in TDD wireless systems where the BS has imperfect knowledge of the channel. The problem in this thesis was minimizing the power consumption at the BS while satisfying the QoS requirements of the users in the network with certain probability. This problem is particularly relevant in the wireless applications that require fixed-rate low-latency communication. Although the designed problem itself is one for which it is difficult to find the optimal solution, several methods were proposed to finding power loadings that satisfy the QoS requirements and have low power consumption.

First, a general purpose algorithm was proposed. This algorithm tackles the problem directly, without any approximation, and is applicable for any arbitrary fixed-direction beamforming, and showed good performance in different scenarios. As the problem becomes harder, e.g., with higher QoS requirements or larger CSI uncertainty

size, the advantages of this method over the existing methods become quite apparent. In fact, even though this method employs fixed beamforming directions that are based on the channel estimates, it provided better performance than the state-of-the-art method that designs the beamformers and the power allocation jointly. The reason for the good performance is that the proposed method tackles the problem directly, without conservative approximation. The difficulty with proposed general method was the computational cost of evaluating several integrals numerically.

To address the issue of computational cost, some other robust power loading algorithms were proposed for the special case in which the beamforming directions were chosen to be zero-forcing directions. In the case, the approximations that were employed to propose those algorithms degraded, to some degree, the performance in comparison to the general proposed method, but they reduce the computational cost dramatically. Even these comparatively computationally cheap methods performed better than the existing conservative methods in difficult scenarios.

In summary, the experiments of this thesis suggest that by tackling the power loading problem directly (or closely), even with suboptimal algorithms, we may be able to obtain better performance rather than the existing robust power loading and even robust precoding methods which are based on optimal solutions to tractable conservative approximations of the problem.

6.2 Future Work

The work in this thesis is based on a number of modelling assumptions, and there is considerable potential for future work in the relaxation of some of these assumptions.

The most important assumption was assuming to have a TDD system. This enabled us to model the channel uncertainty as being Gaussian and hence enabled us to exploit the results of Al-Naffouri and Hassibi (2009). In FDD systems, the acquisition of CSI at the transmitter involves a quantization procedure, and the resulting channel uncertainty can not be actually modeled as being Gaussian (Caire *et al.*, 2010). Therefore, for FDD systems, there is a need to develop a method to express the outage constraint as a deterministic constraint. If that can be done the basic principles of the proposed approach can be applied.

Another issue that could be addressed in future work is that all the computationally cheap algorithms in this thesis are based on ZF beamforming. There is a possibility that the integral expression for the outage probability with an arbitrary beamformer could be approximated in a way that might also enable the application of residue theory. If that were possible, we might be able to propose algorithms that are numerically cheaper than the general algorithms for arbitrary beamformers that were proposed in Chapter 3 of this thesis.

The focus of this thesis was on MISO downlink of single-cell. Generalizing the proposed algorithms in the case of cooperative base stations in the multi-cell schemes with a single antenna at each receiver appears may well be possible, so long as the Gaussian assumption on the error in the transmitter channel state estimates can be justified. In the single-cell case extensions to the case of systems with multiple antennas at the receiver are reasonably straightforward if the transmitter sends only one data stream to each user or if it uses same orthogonal space-time block coding. In those cases, the receiver's QoS can still be specified in terms of a scalar SINR. The case of systems that send multiple data streams to each user is significantly more

difficult, even in the case in which the transmitter has perfect CSI.

Finally, we went on the possibility of tackling directly the robust precoding problem, in which there is the extra degree of freedom of choosing the directions of beamformers, rather than just the robust power loading problem considered in this thesis. These extra degrees of freedom have the potential to significantly improve the performance.

Appendix A

Proof of Lemma 1

Let $\mathbf{Q}$ be a deterministic Hermitian symmetric matrix of size $M \times M$ and consider the non-central quadratic form

$$\|\mathbf{x}-\mathbf{a}\|_{\mathbf{Q}}^2 = (\mathbf{x}-\mathbf{a})^H \mathbf{Q}(\mathbf{x}-\mathbf{a}), \tag{A.1}$$

where $\mathbf{a}$ is a deterministic vector and $\mathbf{x}$ is a standard circular complex Gaussian random vector; i.e., $\mathbf{x} \sim CN(\mathbf{0}, \mathbf{I})$. The cumulative density function (CDF) of $\|\mathbf{x}-\mathbf{a}\|_{\mathbf{Q}}^2$ is given by

$$\Pr\big(\|\mathbf{x}-\mathbf{a}\|_{\mathbf{Q}}^2 < \tau\big) = \int_{\mathcal{A}} p(\mathbf{x}) d\mathbf{x}, \tag{A.2}$$

where $\mathcal{A}$ is the volume in $\mathbb{C}^M$ defined by $\|\mathbf{x}-\mathbf{a}\|_{\mathbf{Q}}^2 < \tau$. Therefore, we can rewrite (A.2) as

$$\Pr\big(\|\mathbf{x}-\mathbf{a}\|_{\mathbf{Q}}^2 < \tau\big) = \frac{1}{\pi^M} \int_{-\infty}^{+\infty} e^{-\|\mathbf{x}\|^2} u(\tau - \|\mathbf{x}-\mathbf{a}\|_{\mathbf{Q}}^2) d\mathbf{x}, \tag{A.3}$$

where $u(\cdot)$ is the unit step function.

To simplify (A.3), the unit step is replaced by its Fourier transform

$$u(z) = \frac{1}{2\pi}\int_{-\infty}^{+\infty} \frac{e^{z(i\omega+\beta)}}{i\omega+\beta} d\omega, \tag{A.4}$$

which is valid for any $\beta > 0$. By substituting (A.4) into (A.3) and reordering the integrals, the CDF can be written as

$$\Pr\big(\|\mathbf{x}-\mathbf{a}\|_{\mathbf{Q}}^2 < \tau\big) = \frac{1}{2\pi^{M+1}}\int_{-\infty}^{+\infty} \frac{e^{\tau(i\omega+\beta)}}{i\omega+\beta} d\omega \underbrace{\int e^{-\overbrace{\big(\|\mathbf{x}\|^2 + (i\omega+\beta)\|\mathbf{x}-\mathbf{a}\|_{\mathbf{Q}}^2\big)}^{A_1}} d\mathbf{x}}_{I_1}. \tag{A.5}$$

The inner integral, I_1, can be simplified by following steps. Denoting $s = i\omega + \beta$, we can rewrite the argument of the exponential in the integrand, A_1, as

$$A_1 = \mathbf{x}^H\big(\mathbf{I}+s\mathbf{Q}\big)\mathbf{x} - s\mathbf{x}^H\mathbf{Q}\mathbf{a} - s\mathbf{a}^H\mathbf{Q}\mathbf{x} + s\mathbf{a}^H\mathbf{Q}\mathbf{a}. \tag{A.6}$$

Let $\mathbf{Q} = \mathbf{V}\mathbf{\Lambda}\mathbf{V}^H$ denote the eigen-decomposition of $\mathbf{Q}$. The term A_1 can then be written as

$$A_1 = \tilde{\mathbf{x}}^H\big(\mathbf{I}+s\mathbf{\Lambda}\big)\tilde{\mathbf{x}} - s\tilde{\mathbf{x}}^H\mathbf{\Lambda}\tilde{\mathbf{a}} - s\tilde{\mathbf{a}}^H\mathbf{\Lambda}\tilde{\mathbf{x}} + s\tilde{\mathbf{a}}^H\mathbf{\Lambda}\tilde{\mathbf{a}}, \tag{A.7}$$

where $\tilde{\mathbf{x}} = \mathbf{V}^H\mathbf{x}$ and $\tilde{\mathbf{a}} = \mathbf{V}^H\mathbf{a}$. Since $\mathbf{V}$ is unitary

$$d\tilde{\mathbf{x}} = |\det(\mathbf{V}^H)|^2 d\mathbf{x} = d\mathbf{x}, \tag{A.8}$$

and by using the results of (A.7) and the fact that $\tilde{\mathbf{x}}$ is also a standard complex

Gaussian random vector, i.e., $\tilde{\mathbf{x}} \in CN(\mathbf{0}, \mathbf{I})$, I_1 can be decomposed as

$$I_1 = \prod_{m=1}^{M} \underbrace{\int_{-\infty}^{+\infty} e^{-\left((1+\lambda_m s)|\tilde{x}_m|^2 - s\lambda_m(\tilde{x}_m^* \tilde{a}_m + \tilde{a}_m^* \tilde{x}_m) + s\lambda_m |\tilde{a}_m|^2\right)} d\tilde{x}_m}_{I_2}, \tag{A.9}$$

where λ_m denotes the eigenvalues of $\mathbf{Q}$ in descending order, and $\tilde{x}_m$ and $\tilde{a}_m$ are the m^{th} elements of vector $\tilde{\mathbf{x}}$ and $\tilde{\mathbf{a}}$, respectively.

In the next step we will decompose the integral in (A.9) over the complex variable $\tilde{x}_m$ into two integrals over real variables $\tilde{x}_m^{\mathrm{Re}}$ and $\tilde{x}_m^{\mathrm{Im}}$, where $\tilde{x}_m = \tilde{x}_m^{\mathrm{Re}} + i\tilde{x}_m^{\mathrm{Im}}$. This is possible because $\tilde{\mathbf{x}}$ (and $\mathbf{x}$) are circular. Then, by completing the squares for each variable, we can rewrite I_2 as

$$I_2 = e^{-c_m} \int_{-\infty}^{+\infty} e^{-(1+s\lambda_m)\left(\tilde{x}_m^{\mathrm{Re}} - \frac{s\lambda_m}{1+s\lambda_m}\tilde{a}_m^{\mathrm{Re}}\right)^2} d\tilde{x}_m^{\mathrm{Re}} \int_{-\infty}^{+\infty} e^{-(1+s\lambda_m)\left(\tilde{x}_m^{\mathrm{Im}} - \frac{s\lambda_m}{1+s\lambda_m}\tilde{a}_m^{\mathrm{Im}}\right)^2} d\tilde{x}_m^{\mathrm{Im}}, \tag{A.10}$$

where $\tilde{a}_m = \tilde{a}_m^{\mathrm{Re}} + i\tilde{a}_m^{\mathrm{Im}}$ and $c_m = \frac{|\tilde{a}_m|^2 s\lambda_m}{1+s\lambda_m}$. If we choose $\mathrm{Re}(s) = \beta$ such that $1 + \beta\lambda_m > 0$ for all m, I_2 can be simplified to

$$I_2 = e^{-c_m} \frac{\pi^{1/2}}{(1+s\lambda_m)^{1/2}} \frac{\pi^{1/2}}{(1+s\lambda_m)^{1/2}} = \frac{\pi e^{-c_m}}{(1+s\lambda_m)}. \tag{A.11}$$

By substituting I_2 from (A.11) in (A.9), I_1 can be simplified to

$$I_1 = \prod_{m=1}^{M} \frac{\pi e^{-c_m}}{(1+s\lambda_m)} = \frac{\pi^M e^{-\sum_m c_m}}{\prod_m (1+s\lambda_m)} = \frac{\pi^M e^{-c}}{\det\left(\mathbf{I} + (i\omega+\beta)\mathbf{Q}\right)}, \tag{A.12}$$

where $c = \sum_{m=1}^{M} \frac{|\tilde{a}_m|^2 (i\omega+\beta)\lambda_m}{1+(i\omega+\beta)\lambda_m}$. Substituting (A.12) into (A.5), the proof for Lemma 1

is completed, i.e.,

$$\Pr\big(\|\mathbf{x}-\mathbf{a}\|_{\mathbf{Q}}^2 < \tau\big) = \frac{1}{2\pi}\int_{-\infty}^{\infty} \frac{e^{\tau(i\omega+\beta)}}{i\omega+\beta}\frac{e^{-c}}{\det(\mathbf{I}+(i\omega+\beta)\mathbf{Q})}d\omega. \tag{A.13}$$

Appendix B

Proof of Lower Bound on Actual Probability of Success by Solving the Approximated Problem

Let $Y(\boldsymbol{\delta}_k) = \boldsymbol{\delta}_k^H \mathbf{Q}_k \boldsymbol{\delta}_k + v_k$ and $X(\boldsymbol{\delta}_k) = (\frac{p_k}{\gamma_k}) 2\,\mathrm{Re}(\boldsymbol{\delta}_k^H \tilde{\mathbf{r}}_k)$, so we can rewrite the actual probability of success as

$$\Pr\Big(X(\boldsymbol{\delta}_k) + Y(\boldsymbol{\delta}_k) \geq 0\Big) = \int_{\mathbb{C}^{N_t}} f(\boldsymbol{\delta}_k) u\Big(X(\boldsymbol{\delta}_k) + Y(\boldsymbol{\delta}_k)\Big) d\boldsymbol{\delta}_k, \tag{B.14}$$

where $f(\boldsymbol{\delta}_k)$ is the probability density function for $\boldsymbol{\delta}_k$ and $u(\cdot)$ is the unit step function. Let us define two sets, $\mathcal{B}_1$ and $\mathcal{B}_2$, where $\mathcal{B}_1$ is the volume in which $X(\boldsymbol{\delta}_k) \geq \frac{p_k}{\gamma_k}\eta_k$ and $\mathcal{B}_2$ is the volume in which $X(\boldsymbol{\delta}_k) < \frac{p_k}{\gamma_k}\eta_k$. Since $\mathcal{B}_1 \cap \mathcal{B}_2 = \emptyset$ and $\mathcal{B}_1 \cup \mathcal{B}_2 = \mathbb{C}^{N_t}$, these

two sets form a partition of $\mathbb{C}^{N_t}$. Therefore, the integral in (B.14) can be written as

$$\int_{\mathcal{B}_1} f(\boldsymbol{\delta}_k) u\Big(X(\boldsymbol{\delta}_k) + Y(\boldsymbol{\delta}_k)\Big) d\boldsymbol{\delta}_k + \underbrace{\int_{\mathcal{B}_2} f(\boldsymbol{\delta}_k) u\Big(X(\boldsymbol{\delta}_k) + Y(\boldsymbol{\delta}_k)\Big) d\boldsymbol{\delta}_k}_{I'(\eta_k)}. \tag{B.15}$$

Considering the fact that in the set $\mathcal{B}_1$, $X(\boldsymbol{\delta}_k) \geq \frac{p_k}{\gamma_k}\eta_k$, we can construct a lower-bound for the integral over set $\mathcal{B}_1$ in (B.15) by replacing $X(\boldsymbol{\delta}_k)$ by $\frac{p_k}{\gamma_k}\eta_k$; i.e.,

$$\int_{\mathcal{B}_1} f(\boldsymbol{\delta}_k) u\Big(X(\boldsymbol{\delta}_k) + Y(\boldsymbol{\delta}_k)\Big) d\boldsymbol{\delta}_k \geq \int_{\mathcal{B}_1} f(\boldsymbol{\delta}_k) u\Big(\tfrac{p_k}{\gamma_k}\eta_k + Y(\boldsymbol{\delta}_k)\Big) d\boldsymbol{\delta}_k. \tag{B.16}$$

Now, lets look at the probability of success for the approximated problem, i.e., $\Pr\Big(\frac{p_k}{\gamma_k}\eta_k + Y(\boldsymbol{\delta}_k) \geq 0\Big)$. By taking the same steps we can reformulate this probability as

$$\Pr\Big(\tfrac{p_k}{\gamma_k}\eta_k + Y(\boldsymbol{\delta}_k) \geq 0\Big) \tag{B.17a}$$

$$= \int_{\mathbb{C}^{N_t}} f(\boldsymbol{\delta}_k) u\Big(\tfrac{p_k}{\gamma_k}\eta_k + Y(\boldsymbol{\delta}_k)\Big) d\boldsymbol{\delta}_k \tag{B.17b}$$

$$= \int_{\mathcal{B}_1} f(\boldsymbol{\delta}_k) u\Big(\tfrac{p_k}{\gamma_k}\eta_k + Y(\boldsymbol{\delta}_k)\Big) d\boldsymbol{\delta}_k + \int_{\mathcal{B}_2} f(\boldsymbol{\delta}_k) u\Big(\tfrac{p_k}{\gamma_k}\eta_k + Y(\boldsymbol{\delta}_k)\Big) d\boldsymbol{\delta}_k \tag{B.17c}$$

Now recall that $\rho_k(\eta_k)$ was defined such that

$$\rho_k(\eta_k) = \Pr\big(2\,\mathrm{Re}(\boldsymbol{\delta}_k^H \tilde{\mathbf{r}}_k) \geq \eta_k\big) = \Pr\big(X(\boldsymbol{\delta}_k) \geq \tfrac{p_k}{\gamma_k}\eta_k\big). \tag{B.18}$$

The second integral in (B.17c) has an upper bound, $1-\rho_k(\eta_k)$, since if the step function was equal to one over the volume $\mathcal{B}_2$, this integral would be equal to $1-\rho_k(\eta_k)$. Using

this result, we have

$$\int_{\mathcal{B}_1} f(\boldsymbol{\delta}_k) u\Big(\tfrac{p_k}{\gamma_k}\eta_k + Y(\boldsymbol{\delta}_k)\Big) d\boldsymbol{\delta}_k \geq \Pr\Big(\tfrac{p_k}{\gamma_k}\eta_k + Y(\boldsymbol{\delta}_k) \geq 0\Big) - \big(1 - \rho_k(\eta_k)\big). \tag{B.19}$$

Now in the approximated problem in Section 4.1, we design the system so that $\Pr\Big(\frac{p_k}{\gamma_k}\eta_k + Y(\boldsymbol{\delta}_k) \geq 0\Big) \geq 1 - \epsilon_k$. Therefore, in that case we have

$$\int_{\mathcal{B}_1} f(\boldsymbol{\delta}_k) u\Big(\tfrac{p_k}{\gamma_k}\eta_k + Y(\boldsymbol{\delta}_k)\Big) d\boldsymbol{\delta}_k \geq 1 - \epsilon_k - \big(1 - \rho_k(\eta_k)\big) = \rho_k(\eta_k) - \epsilon_k. \tag{B.20}$$

Substituting the result back into (B.16) we have

$$\Pr\Big(X(\boldsymbol{\delta}_k) + Y(\boldsymbol{\delta}_k) \geq 0\Big) \geq \rho_k(\eta_k) - \epsilon_k + I'(\eta_k). \tag{B.21}$$

Appendix C

Performance Analysis Against η_k

In this appendix, we numerically evaluate the effect of η_k on approximated problem in (4.4) and also on the actual feasibility rate. With this goal in mind, we consider an environment in which $N_t = K = 3$, $\gamma_k = \gamma = 3$ dB, $\sigma_k^2 = \sigma^2 = 0.01$ and $\epsilon_k = \epsilon = 0.05$. We randomly generated 10,000 realizations of the set of i.i.d. Rayleigh fading channels $\{\mathbf{h}_k^H\}_{k=1}^K$. Then, we determined channel estimates at the BS by using the uplink training scheme for TDD systems that results in $\mathbf{C}_k = \mathbf{C} = 0.002\mathbf{I}$; c.f., Chapter 2.

It is more convenient to express η_k as $\eta_k = -\eta_k' \times 2\|\tilde{\mathbf{r}}\|$ and then consider the value of η_k'. In our implementation, we assume that η_k' is equal for all users; i.e., $\eta_k' = \eta'$. In Fig. C.1 the feasibility rate for approximated problem is shown; i.e., the percentage of instance in which the algorithm is successful to solve the approximated problem corresponding to that η'. It can be seen that smaller η' results in simpler problem to solve; hence, the algorithm produces feasible solution more often.

As the problem of real interest is the original problem, in Fig. C.2, the actual feasibility rate, which is the percentage of instance in which the algorithm is successful

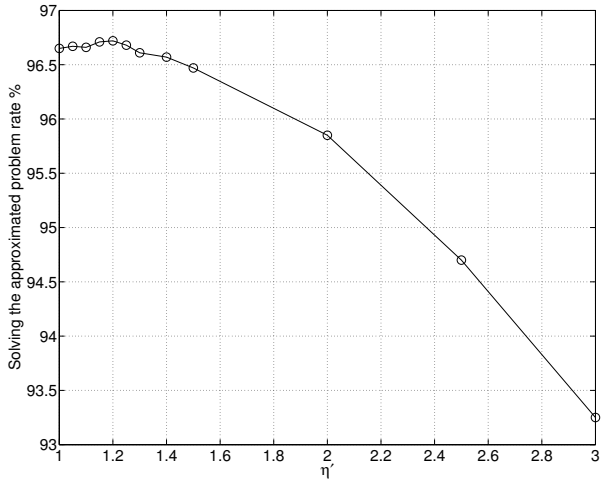

Figure C.1: Feasibility rate of approximated problem against η' in the environment where $N_t = K = 3$, $\mathbf{C} = 0.002\mathbf{I}$, $\sigma^2 = 0.01$, $\epsilon = 0.05$, $\gamma = 3$ dB.

to solve the original problem is shown. It can be seen in Fig. C.2 that for $\eta' < 1.15$, the algorithm is not able to solve the original problem very often. However, for slightly larger values of η' the feasibility rate improves dramatically. For still larger value of η', the feasibility rate decreases slowly. This is expected because the approximated problem becomes incesaingly conservative as η'_k increases.

In implementing a fixed η' algorithm in our simulations, we set $\eta' = 1.3$ which is a reasonable choice according to the results of this section.

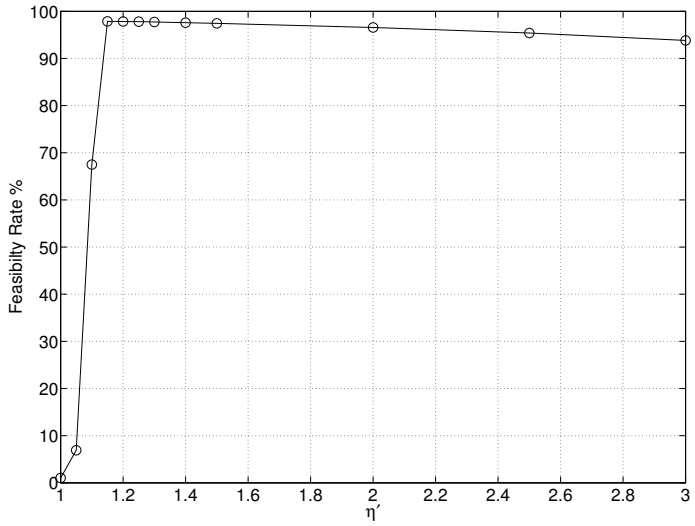

Figure C.2: Actual feasibility rate against η' in the environment where $N_t = K = 3$, $\mathbf{C} = 0.002\mathbf{I}$, $\sigma^2 = 0.01$, $\epsilon = 0.05$, $\gamma = 3$ dB.

Appendix D

Algorithm for Changing η_k

In Section 4.5, an iterative process was suggested for the selection of the parameter η_k. This process suggested that when the actual probability that the SINR target is achieved was not satisfied, η_k' should be increased, and when the SINR target is over-satisfied, η_k' should be decreased. In Algorithm 3, we provide an explicit statement of how the principals were implemented in the experiments described in Chapter 5.

Algorithm 3 Choosing the η_k at the i^{th} iteration on η_k; $\eta_k^{(i)}$

Calculate $S_k = \Pr\big(\mathsf{SINR}_k \geq \gamma_k\big)$ using the integral in (4.5b)
for $k = 1 \rightarrow K$ **do**
    if $0.99 \leq S_k$ **then**
        $\eta_k^{(i)} = 0.5 \times \eta_k^{(i-1)}$
    else if $0.97 \leq S_k < 0.99$ **then**
        $\eta_k^{(i)} = 0.7 \times \eta_k^{(i-1)}$
    else if $0.96 \leq S_k < 0.97$ **then**
        $\eta_k^{(i)} = 0.9 \times \eta_k^{(i-1)}$
    else if $0.955 \leq S_k < 0.96$ **then**
        $\eta_k^{(i)} = 0.97 \times \eta_k^{(i-1)}$
    else if $0.945 \leq S_k < 0.95$ **then**
        $\eta_k^{(i)} = 1.03 \times \eta_k^{(i-1)}$
    else if $0.93 \leq S_k < 0.945$ **then**
        $\eta_k^{(i)} = 1.1 \times \eta_k^{(i-1)}$
    else if $0.90 \leq S_k < 0.93$ **then**
        $\eta_k^{(i)} = 1.3 \times \eta_k^{(i-1)}$
    else if $S_k < 0.90$ **then**
        $\eta_k^{(i)} = 1.5 \times \eta_k^{(i-1)}$
    end if
end for

Appendix E

Performance of the Proposed User Selection Heuristic

In this appendix, we compare the performance of systems without user selection module, those that employ a simple heuristic of user selection and the exhaustive search approach to finding the optimal user selection for the proposed power allocation algorithm. With this in mind, we consider an environment with four users, of which the BS will transmit to $K = 3$ where the other parameters are set to be $N_t = 3$, $\sigma_e^2 = 0.002$, $\sigma^2 = 0.01$ and $\epsilon = 0.05$. We find the feasibility rate and transmission power over 1,000 channel realization for the general algorithm proposed in Chapter 3 with ZF beamforming direction.

The system without user selection module always picks the first three users. The system with heuristic user selection eliminates the user with the smaller channel estimate norm among the pair of users that have the maximum inner product of the channel estimates. Finally, the best user selection scheme is obtained by exhaustive search among all sets of possible choices of three users and picking the set for which

the algorithm produces the feasible beamformer with the smallest transmission power.

The results for this simulation are illustrated in Fig. E.3 and Fig. E.4. It can be seen that even with the simple heuristic user selection the improvement of performance is considerable. However, user selection with exhaustive search results in much better performance.

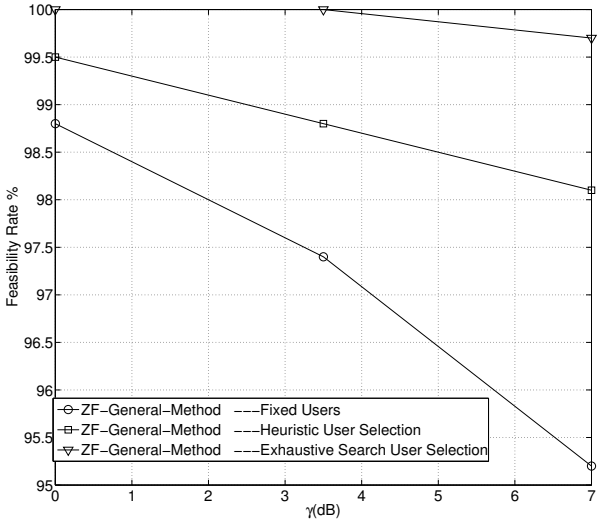

Figure E.3: Feasibility rate in the environment where $N_t = 3$, $\mathbf{C} = 0.002\mathbf{I}$, $\sigma^2 = 0.01$, $\epsilon = 0.05$ and the BS should communicate to $K = 3$ users of four users available in the network.

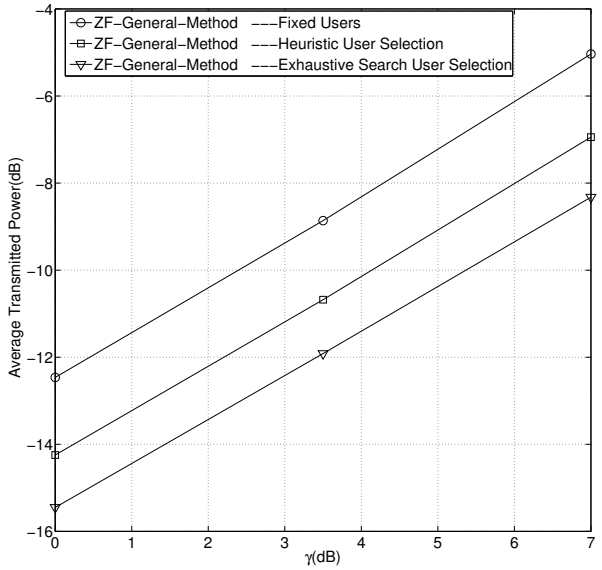

Figure E.4: Average transmission power in the environment where $N_t = 3$, $\mathbf{C} = 0.002\mathbf{I}$, $\sigma^2 = 0.01$, $\epsilon = 0.05$ and the BS should communicate to $K = 3$ users of four users available in the network.

Bibliography

Al-Naffouri, T. Y. and Hassibi, B. (2009). On the distribution of indefinite quadratic forms in Gaussian random variables. In *Proc. Int. Symp. Info. Theory*, pages 1744–1748, Seoul.

Bengtsson, M. and Ottersten, B. (2001). Optimal and suboptimal transmit beamforming. In L. C. Godara, editor, *Handbook of Antennas in Wireless Communications*, chapter 18. CRC Press.

Bertsekas, D. P. (1999). *Nonlinear Programming*. Athena Scientific, Belmont, MA, second edition.

Botros Shenouda, M. and Davidson, T. N. (2007). Convex conic formulations of robust downlink precoder design with quality of service constraints. *IEEE J. Sel. Topics Signal Process.*, **1**(4), 714–724.

Botros Shenouda, M. and Davidson, T. N. (2008). Probabilistically-constrained approaches to the design of the multiple antenna downlink. In *Conf. Rec. 42nd Ann. Asilomar Conf. Signals, Systems, Computers*, pages 1120–1124, Pacific Grove, CA.

Botros Shenouda, M. and Davidson, T. N. (2009). Non-linear and linear broadcasting

with QoS requirements: Tractable approaches for bounded channel uncertainties. *IEEE Trans. Signal Process.*, **57**(5), 1936–1947.

Caire, G. and Shamai, S. (2003). On the achievable throughput of a multiantenna Gaussian broadcast channel. *IEEE Trans. Inf. Theory*, **49**(7), 1691–1706.

Caire, G., Jindal, N., Kobayashi, M., and Ravindran, N. (2010). Multiuser MIMO achievable rates with downlink training and channel state feedback. *IEEE Trans. Info. Theory*, **56**(6), 2845–2866.

Chalise, B., Shahbazpanahi, S., Czylwik, A., and Gershman, A. B. (2007). Robust downlink beamforming based on outage probability specifications. *IEEE Trans. Wireless Commun.*, **6**(10), 3498–3503.

Fung, C.-H., Yu, W., and Lim, T. J. (2007). Precoding for the multiantenna downlink: Multiuser SNR gap and optimal user ordering. *IEEE Trans. Commun.*, **55**(1), 188–197.

Gesbert, D., Kountouris, M., Heath, R. W., Chae, C.-B., and Salzer, T. (2007). Shifting the MIMO paradigm. *IEEE Signal Process. Mag.*, **24**(5), 36–46.

Gesbert, D., Hanly, S., Huang, H., Shamai Shitz, S., Simeone, O., and Yu, W. (2010). Multi-cell MIMO cooperative networks: A new look at interference. *IEEE J. Sel. Areas Commun.*, **28**(9), 1380–1408.

Goldsmith, A. (2005). *Wireless communications*. Cambridge University Press.

Grant, M. and Boyd, S. (2012). CVX: MATLAB software for disciplined convex programming, version 2.0 beta. `http://cvxr.com/cvx`.

Hassibi, B. and Hochwald, B. M. (2003). How much training is needed in multiple-antenna wireless links? *IEEE Trans. Inf. Theory*, **49**(4), 951–963.

Hochwald, B. M., Peel, C. B., and Swindlehurst, A. L. (2005). A vector-perturbation technique for near-capacity multiantenna multiuser communication-part II: Perturbation. *IEEE Trans. Wireless Commun.*, **53**(3), 537–544.

Huang, Y. and Palomar, D. P. (2010). Rank-constrained separable semidefinite programming with applications to optimal beamforming. *IEEE Trans. Signal Process.*, **58**(2), 664–678.

Hunger, R. and Joham, M. (2010). A complete description of the QoS feasibility region in the vector broadcast channel. *IEEE Trans. Signal Process.*, **58**(7), 3870–3878.

Jindal, N. (2006). MIMO broadcast channels with finite-rate feedback. *IEEE Trans. Inf. Theory*, **52**(11), 5045–5060.

Jindal, N., Lozano, A., and Marzetta, T. L. (2009). What is the value of joint processing of pilots and data in block-fading channels? In *Proc. IEEE Int. Symp. Inf. Theory*, pages 2189–2193, Seoul.

Kaltenberger, F., Jiang, H., Guillaud, M., and Knopp, R. (2010). Relative channel reciprocity calibration in MIMO/TDD systems. In *Proc. Future Network and Mobile Summit, 2010*, pages 1–10.

Lapidoth, A. and Shamai, S. (2002). Fading channels: How perfect need perfect side information be? *IEEE Trans. Inf. Theory*, **48**(5), 1118–1134.

Liu, J. and Krzymien, W. A. (2008). A novel nonlinear joint transmitter-receiver

processing algorithm for the downlink of multiuser MIMO systems. *IEEE Trans. Veh. Technol.*, **57**(4), 2189–2204.

Park, J., Sung, Y., Kim, D., and Poor, H. V. (2012). Outage probability and outage-based robust beamforming for MIMO interference channels with imperfect channel state information. *IEEE Trans. Wireless Commun.*, **11**(10), 3561–3573.

Payaró, M., Pascual-Iserte, A., and Lagunas, M. Á. (2007). Robust power allocation designs for multiuser and multiantenna downlink communication systems through convex optimization. *IEEE J. Sel. Areas Commun.*, **25**(7), 1390–1401.

Peel, C. B., Hochwald, B. M., and Swindlehurst, A. L. (2005). A vector-perturbation technique for near-capacity multiantenna multiuser communication–Part I: Channel inversion and regularization. *IEEE Trans. Commun.*, **53**(1), 195–202.

Poor, H. V. (1994). *An introduction to signal detection and estimation.* Springer-Verlag New York, Inc., New York, NY, USA, second edition.

Rashid-Farrokhi, F., Tassiulas, L., and Liu, K. J. R. (1998). Joint optimal power control and beamforming in wireless networks using antenna arrays. *IEEE Trans. Commun.*, **46**(10), 1313–1324.

Salim, U., Gesbert, D., and Slock, D. (2012). Combining training and quantized feedback in multiantenna reciprocal channels. *IEEE Trans. Signal Process.*, **60**(3), 1383–1396.

Schubert, M. and Boche, H. (2007). A generic approach to QoS-based transceiver optimization. *IEEE Trans. Commun.*, **55**(8), 1557–1566.

Smith, G. S. (2004). A direct derivation of a single-antenna reciprocity relation for the time domain. *IEEE Trans. Antennas Propag.*, **52**(6), 1568–1577.

Sohrabi, F. and Davidson, T. N. (2013). Coordinate update algorithms for robust power loading for the MISO downlink with outage constraints and Gaussian uncertainties. In *Proc. Int. Conf. Acoust., Speech, Signal Process.*, pages 4769–4773, Vancouver.

Spencer, Q. H., Swindlehurst, A. L., and Haardt, M. (2004). Zero-forcing methods for downlink spatial multiplexing in multiuser MIMO channels. *IEEE Trans. Signal Process.*, **52**(2), 461–471.

Tse, D. and Viswanath, P. (2005). *Fundamentals of wireless communication*. Cambridge University Press.

Vucic, N. and Boche, H. (2009). Robust QoS-constrained optimization of dowlink multiuser MISO systems. *IEEE Trans. Signal Process.*, **57**(2), 714–725.

Vučić, N. and Boche, H. (2009). A tractable method for chance-constrained power control in downlink multiuser MISO systems with channel uncertainty. *IEEE Sig. Proc. Lett.*, **16**(5), 346–349.

Wang, K.-Y., Chang, T.-H., Ma, W.-K., So, A. M.-C., and Chi, C.-Y. (2011). Probabilistic SINR constrained robust transmit beamforming: A Bernstein-type inequality based conservative approach. In *Proc. Int. Conf. Acoust., Speech, Signal Process.*, pages 3080–3083, Prague. See also: `http://arxiv.org/abs/1108.0982`.

Weingarten, H., Steinberg, Y., and Shamai, S. (2006). The capacity region of the

Gaussian multiple-input multiple-output broadcast channel. *IEEE Trans. Inf. Theory*, **52**(9), 3936–3964.

Wiesel, A., Eldar, Y., and Shamai, S. (2006). Linear precoding via conic optimization for fixed MIMO receivers. *IEEE Trans. Signal Process.*, **54**(1), 161–176.

Windpassinger, C., Fischer, R. F., Vencel, T., and Huber, J. B. (2004). Precoding in multiantenna and multiuser communications. *IEEE Trans. Wireless Commun.*, **3**(4), 1305–1316.

Winters, J. H., Salz, J., and Gitlin, R. D. (1994). The impact of antenna diversity on the capacity of wireless communication systems. *IEEE Trans. Commun.*, **42**(2/3/4), 1740–1751.

Zheng, G., Wong, K.-K., and Ng, T.-S. (2008). Robust linear MIMO in the downlink: A worst-case optimization with ellipsoidal uncertainty regions. *EURASIP J. Adv. Signal Process.*, **2008**(609018).